JIMMA UNIVERSITY

JIMMA INSTITUTE OF TECHNOLOGY

SCHOOL OF POSTGRADUATE STUDIES

FACULTY OF MATERIALS SCIENCE AND ENGINEERING

Title: Effect of Temperature on Cu (Se, S) for the Degradation of Methylene Blue in Aqueous Solution

A thesis submitted to the School of Graduate Studies of Jimma University for the Partial Fulfillment of the Requirement of Master of Science Degree in Materials Science and Engineering

By: Ribka Habteyesus Tereda

ID No. RU2757-12

October, 2021

Jimma, Ethiopia

JIMMA UNIVERSITY

JIMMA INSTITUTE OF TECHNOLOGY

SCHOOL OF POSTGRADUATE STUDIES

FACULTY OF MATERIALS SCIENCE AND ENGINEERING

Title: Effect of Temperature on Cu (Se, S) for the Degradation of Methylene Blue in Aqueous solution

A thesis submitted to the School of Graduate Studies of Jimma University for the Partial Fulfillment of the Requirement of Master of Science Degree in Materials Science and Engineering

Advisors:

- Main Advisor: Dr. Dinsefa Mensure Andoshe, Department of Materials Science and Engineering, Adama Science and Technology University (ASTU)
- Co-Advisor: Dr. Olu Emmanuel Femi, Jimma University, JIT

DECLARATION

This is to declare that this research work, which is done and having the title Effect of Temperature on Cu (Se, S) for the Degradation of Methylene Blue in Aqueous Solution is my original work. The appropriate credit has been given where reference has been made to the work of others. All referenced parts have been used to argue the idea and have been cited properly. I will be responsible and liable for any consequence if a violation of this declaration is proven. I submit this research work to Jimma Institute of Technology in partial fulfillment of the requirement for the award of the degree of Master of Science in Materials Science and Engineering.

Name: Ribka Habteyesus Tereda

Signature: _____Date of submission: _____

This thesis has been submitted with my approval as an advisor

1. Dr. Dinsefa Mensure (Main Advisor)

Signature: _____ Date: _____

2. Dr. Olu Emmanuel Femi (Co-Advisor)

Signature: _____ Date: _____

Examiner: _____ Signature: _____ Date: _____

Faculty approval

Abstract

Water pollution is one of the biggest problems in the world nowadays. Among various contaminants at about 20% of the water pollution is caused by organic dyes. Organic dye removal from different sources has never been easy and is becoming a major concern for environmental and societal health. Among these organic dyes, cationic methylene blue is highly toxic and can cause great environmental pollution and health effects. In this work, the effect of temperature on sulfur doped copper selenide for degradation of methylene blue was studied. Initially, Cu (Se, S) was synthesized by the hydrothermal method, then the synthesized materials were characterized using X-Ray Diffraction, Scanning Electron Microscopy, Fourier Transform-Infra Red Spectroscopy, Photoluminescence spectroscopy, and UV-Vis Diffuse Reflectance Spectroscopy to determine phase purity, the particles morphology, functional groups, photon recombination, and the degradation efficiency respectively. From the diffraction pattern, it is confirmed the synthesized CuSe was crystalline klomannite hexagonal with no other impurities peaks and Scanning Electron Microscope reveals that *synthesized pristine CuSe with smooth surface and relatively symmetrical hexagonal shapes. The optical bandgap of the synthesized samples CuSe, 3% S CuSe, and 5% S CuSe estimated from Diffuse Reflectance Spectroscopy and Photoluminescence spectroscopy measurement were becoming 2.33eV,2.3eV, 2.32eV respectively. 3% S CuSe exhibited a better degradation efficiency of about 46.5% at the initial MB concentration of 10 mg$L^{-1}$and with a catalyst dose of 0.05g. This sample was subsequently selected for further temperature studies. The effect of temperature was investigated for the present material ranging from room temperature to 90℃. At a temperature of 70℃, the degradation efficiency is maximum, with the corresponding results of 70% removal of MB, and decrease at 90℃. The kinetic behavior obeyed the Pseudo-first-order degradation kinetics. Finally, the reusability of the present synthesized material was studied for up to 4 cycles and showed suitable reusability towards the MB removal. Therefore, the results of this study indicate that system temperature has a great effect on the photocatalytic activity of CuSe for the removal of methylene blue organic dye.*

Key words: Cu (Se, S), Hydrothermal synthesis, Photocatalysis, Temperature effect, wastewater, Methylene blue dye

Acknowledgment

Firstly, I would like to praise and thank God, the Almighty, who has granted countless blessings, knowledge, and opportunity to the writer, so that I have been finally able to accomplish the thesis.

Secondly, I would like to express my special appreciation and thanks to my Advisor Dr. Dinsefa Mensure Andoshe, Department of Materials Science and Engineering, Adama Science and Technology University (ASTU) you have been a tremendous mentor for me. I would like to thank you for encouraging my research and for allowing me to grow as a research scientist. Your advice on both research as well as on my career has been invaluable and I would like to thank my Co-Advisor Dr. Olu Emmanuel Femi, Jimma University, JIT their thorough reading of this thesis and for their helpful comments.

Finally, my deep and sincere gratitude to my family for their continuous and unparalleled love, help, and support. I am forever indebted to my parents for giving me the opportunities and experiences that have made me who I am.

Table of Contents

List of figures

List of tables

List of Abbreviation and Symbols

AOP	Advanced oxidation process
℃	Degree centigrade
CB	Conduction band
CuSe	Copper selenide
CTAB	Cetyltrimethylammonium bromide
DRS	Diffused Reflectance Spectroscopy
e^{--}	Electron
Eg	Energy band gap
FTIR	Fourier Transform Infrared
h	Hour
h^+	Holes
H_2O	Water
H_2O_2	Hydrogen peroxide
HO_2	Perhydroxyl radical
hν	Photon
KBr	Potassium bromide
NaOH	Sodium hydroxide
$O_2\cdot$	Super oxide radical
OH	Hydroxyl radical
S	Sulfur
Sec	Second
UV-Vis	Ultra violet visible
v	Frequency
VB	Valence band
XRD	X-ray diffraction
η	Efficiency

θ	Diffraction angle
pH	pH value

CHAPTER ONE

1. Introduction

1.1. Background of the study

Water is a vital constituent of a natural resource that has an important role for all living things. About 75 % of the earth is covered by water. Therefore, it is impossible to imagine life without water [3]. Currently, because of economic development and population growth, the demand for freshwater is increasing. The health of humans and other organisms is directly related to clean water other than anything. Water has been applied in numerous human deeds for plenty of functions consisting of agriculture, industry, home, and electricity production. Globally, home uses 15% of the whole water consumption; at, the same time, about 25% is utilized in commercial sports and 60% in agriculture [4]. However, the commercial wastewater streams pose a severe risk to human existence, plants, and animals. One of the essential assets of groundwater and floor water pollutants is commercial effluents from textile, pulp, and paper, pharmaceutical, and different chemical industries [5]. Nowadays, water resources are full of untreated waste materials, discharge of hazardous and toxic dyes; because, of these industrial wastewater effluents, environmental pollution is one of the significant challenges in the world till now, which is needed to be considered. About 420 billion liters of sewage are discharged into water resources every year, which is at about 14 percent of the total drinking water of the earth. Moreover, around 4 billion people worldwide have little or no experience with the access of clean and sanitized as well annually millions of people die because of water-borne disease [6] [5].

These Pollutants are classified into two classes based on their boiling point. They include solution pollutants **(dyes)** and insoluble pollutants (oils), which are the primary contaminants in water and wastewaters. Among these water pollutants, dyes are one class of pollutants that greatly affect the environment compared with the others [7]. Textiles industries consume a massive quantity of artificial dyes, about 60% of the production of the whole dye, to present the stylish texture to the cloth materials. Approximately 15% of the dyes undergo tired off unchanged inside the water, which results in a primary reason for environmental pollutants [8].

1.1.2 Dyes

Dyes are natural or synthetic-colored materials used to color various materials. Every year, more than 100,000 types of industrial dyes are used in various textiles, leather, paper, pulp, food processing, and hair dyes. Various chemicals are used for dyeing and printing, so they have an essential role in the textile industry. Wastewater from the dyeing processes is at high temperature and different pH, holding a high amount of the color elements. The release of the dye wastewater into the ecosystem, million cubic meters discharged per year to wastewater treatment systems, is a wonderful source of aesthetic pollution, eutrophication, and perturbation in aquatic life and human life disorders. These affect the respiratory system, nervous system, brain, and liver [7, 9]. Thus, the removal of color from wastewater becomes a challenging problem. Synthetic dyes are difficult to biodegrade because of their complex aromatic nature. Unfortunately, the dyes, mostly azo dyes with aromatic structures, are recalcitrant. The azo dyes are difficult to degrade by aerobic digestion and are steady in oxidizing agents [10].

Classification of Dyes According to Methods of Application

Acid dyes are the sodium salts of coloring acids containing sulfonic and phenolic groups. These are always used in an acidic solution. They directly dye silk and wool (animal fiber). For example, Marzio yellow, orange II, naphthol yellow, etc. Ingrain Dyes These are synthesized in the fiber and can be applied to both animal and plant fibers using a diazotization and coupling process. The color obtained in this type of dye is also called ice color because the diazotization and coupling processes are carried out at low temperatures. Para red is an example of rooted dyes [11].

Basic Dyes are either hydrochloride or zinc chloride complexes of color bases, which are directly used for silk, or wool in basic medium. Azo dyes (Methylene blue) and triphenyl methane dyes are typical examples of this class [12].

Mordent dyes are unable to attach themselves to the fiber. Therefore, they require pretreatment of fiber with a particular substance called mordent‖ like tannin or tannic acid. The mordent gets itself attached to the fiber and then combines with the dye to form an insoluble colored complex. Alizarin, anthraquinone, and azo dyes belong to this class [13].

The Vat Dyes are insoluble in water, but their reduced form is soluble in an alkali solution whereby leuco vat is obtained. The leuco compound is adsorbed on fiber and, upon exposure

to air, is oxidized to the dye, which remains fixed to the cloth. Indigo and anthraquinone vat dyes are good examples of this class [14].

Sulfur Dyes are similar to vat dyes and are sulfur-containing complexes, which are insoluble in water but soluble in a cold alkaline solution of sodium sulfide. They also form leuco complex. These dyes are dark in color, inexpensive, and have good fastness properties. Sulfur black is an example of this class and is used for dyeing cotton [15].

Disperse Dyes are used to dye acetate rayons, Dacron, nylon, and other synthetic fibers. The fiber to be dyed is dipped in a dispersion of finely divided dye in a soap solution in the presence of some solubilizing agent such as phenol, cresol, or benzoic acid. The adsorption onto the fiber is carried out at high 14 temperatures and pressure. An important example of this class is fast pink B and celliton fast blue [16].

Pigment Dyes form insoluble compounds or lakes with salts of Ca, Cr, Ba, Al, or phosphomolybdic acid. These dye molecules contain −OH and $-SO_3H$ groups. Due to their fastness to light, heat, acids, and bases, they are valuable for paints, printing ink, synthetic plastics, fibers, rubbers, etc. Lithol red, pigment red, and acid red are members of pigment dyes [17]. Food Dyes are harmless and used in coloring food, candles, confectionaries, and cosmetics [18].

Methylene Blue (MB)

Among the basic dyes, the methylene blue dye is studied in this work, which is known as basic blue 9 (cationic dye). It is dark blue powder and appears at room temperature. This methylene blue is a common pollutant in sewage industries and textile industries [19]. $C_{16}H_{18}N_3SCl$ is the molecular formula and has 3, 7-bis (dimethylamino) phenthiazin-5-ium chloride IUPAC name. The maximum absorption wavelength of this MB dye is 664 nm [20].

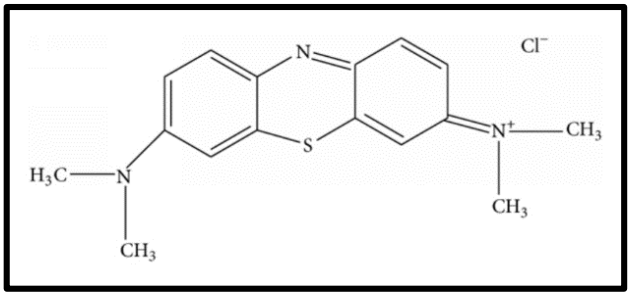

Figure 1: Chemical structure of methylene blue (MB) dye

1.2. Statement of the problem

CuSe is a p-type semiconductor. Due to its physical, chemical, electrical, biochemical, and optical properties, it has potential applications in photocatalysts that degrade organic pollutants. However, this CuSe has poor photocatalytic degradation efficiency of dye molecules in wastewater. Recently, researchers have tried to use a variety of methods to solve these problems, including adding surfactants during the synthesis of nanomaterials to create quantum dots to minimize agglomeration. This thesis focuses on doping sulfur to close the bandgap to entangle and consolidate to increase light absorptive capacity. In addition, study the temperature effect on Cu (Se, S) for the methylene blue degradation because effluents discharged from different industries have different high temperatures and different pH values. As well many factors can significantly affect the photocatalytic reaction, such as concentration, pH value, the grain size of the catalyst, the specific surface area, the morphology of the photocatalyst and the intensity of the incident light are the factors that have been widely studied. So far, but the influence of the system temperature on the photocatalyst has not yet received attention.

1.3. General objective

To study the Effect of Temperature on Cu (Se, S) for the Degradation of Methylene Blue in Aqueous solution.

1.4. Specific objectives

1. To synthesis, the CuSe and sulfur-doped copper selenides using the hydrothermal method.
2. To characterize the synthesized materials by using x-ray diffraction spectroscopy (XRD), Scanning electron microscope (SEM), Fourier transforms infrared spectroscopy (FTIR), Photoluminescence spectroscopy (PL), and UV–vis spectrophotometer.
3. To study the photocatalytic performance of the synthesized material.
4. To study the effect of temperature and doping concentration for the degradation of methylene blue.

1.5. Significance of the Study

Many industrial wastewaters are a toxic result of water pollution, and affect the usage of water and increase the demand for clean water. Among them, the discharge of different dyes from

different industries is a major hazard to the environment. These dyes are very toxic, carcinogenic, which harms living things. Non-biodegradability and high color absorbing properties result in a continuous decrease in aquatic life by blocking sunlight. Organic dyes irritate the respiratory tract, eyes, skin, throat, and allergies. It is essential to degrade the organic pollutants. So photocatalysts are needed due to several advantages such as eco-friendly nature, deodorizing effect, low cost, air purifying, self-cleaning, and water purification. The water treatment process not only produces clean, reusable water, it also has the potential to produce various other benefits for the community. This thesis studied the effect of temperature on sulfur-doped copper selenide photocatalyst for the degradation of methylene blue in aqueous solutions.

CHAPTER TWO

2. Literature review

In this section, we reviewed water purification methods, photocatalysis activity, and parameters that affect the photocatalytic activity. In addition to that, various photocatalysis for the removal of organic dyes from wastewater with a special focus on recent papers have also been reviewed.

2.1. Water Pollution

Water pollution is a contamination of water directly related to industrialization, civilization, and the living standard of people. Water pollutants are physical, chemical, or biological factors causing an aesthetic or detrimental effect on aquatic or those who consume the water [99]. Water pollution has become a significant problem still now. There are exclusive sorts of pollution consisting of non-biodegradable plastic, synthetic chemical, dyes, sludge, and heavy metals [50]. Industries play a great role in the launching of various poisonous chemicals, organic and inorganic sludge, toxic solvents, lead, mercury, nitrates, phosphate, acids, alkaline, dyes, pesticides, benzene, chlorobenzene, carbon tetrachloride, toluene, and volatile organic chemicals [51]. Among various contaminants, dyes have an excellent Vitale legacy of pollution that is discharged into wastewater from textile, dyeing, and different industrial processes, so we want to cast off those dyes, which are vital because of their toxicity, effect of for human, animal, and plants [52].

2.2. Methods for Removal of Dyes from Aqueous Solution

In the past 20 years, conventional wastewater treatment methods have been developed to remove colors from dye-contaminated wastewater, which are divided into three categories as Biological treatment method, physical treatment method, and chemical treatment method. Moreover, flocculation or coagulation, precipitation, filtration, biodegradation, and activated carbon(AC) adsorption are dye removal mechanisms from the waste water [21]. Meanwhile, superior oxidation, adsorption, Biosorption, biomass, and Nanofiltration have emerged as opportunity strategies to supplement the traditional and mounted strategies [22]. These conventional wastewater treatment methods are ineffective in treating these industrial effluents, which contain pollutants those, are highly volatile or not easily absorbable see Figure 2. These methods are applied to treat wastewater, though these methods have limitations. The biological methods have the limitation that it forms a huge amount of biological sludge, which

is difficult to be disposed of. Moreover, the biological method does decrease a negligible amount of pollutants. As well, they need a large earth area and have a complex operational phase [23]. The physical treatment method is also one of the conventional methods but it does not completely degrade the pollutant that they change the phase of the pollutants so that they need post-treatment for regular generation of the adsorbent material. Therefore, transferring the toxic contaminants from one phase to another is not a permanent solution for the treatment of hazardous waste materials [24]. The chemical method has also its drawback which needs a high amount of chemicals for effluent treatment which results in the generation of a huge quantity of sludge and makes it quite expensive for the chemicals as well as for the sludges [25]. Generally, the formation of secondary products, huge manufacturing of sludge, ineffective, costly, and excessive tendency to switch the water pollutant compounds to some other section, have caused the quick improvement of the opportunity method. Somehow, those pollutions have been being focused with the aid of using shifting them to some other section or converting contaminants to different special stages and they will generate secondary pollutants at some point of the regeneration and desorption procedure of saturated adsorbent. Although it's miles hard to degrade natural contaminants with the aid of using those strategies because of their complicated natural structure [26].

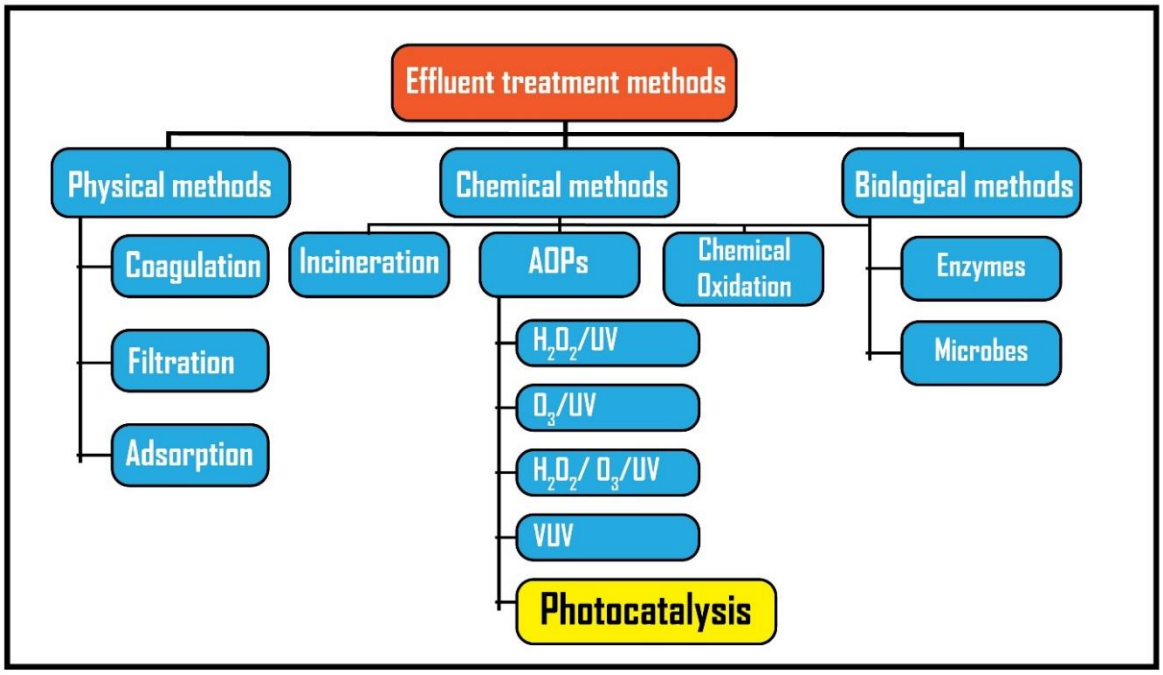

Figure 2: Wastewater treatment Mechanisms [27]

2.3. Advanced oxidation processes (AOPs)

AOPs are recently developed wastewater treatment mechanism involves the generation of in-situ highly reactive oxygen species such as hydroxyl radicals, H_2O_2, O_3, and superoxide anion radicals which aid in the degradation process until the pollutants are completely converted to CO_2, H_2O, and mineral acid [28]. AOPs have been developed rapidly and have different industrial applications [29]. Advanced oxidation processes (AOPs) such as semiconductor photocatalysis, UV/H_2O_2 (Heterogeneous), Fenton, Photo-Fenton, ozonation, and O_3/H_2O_2 (Homogeneous) processes are used for the treatment of recalcitrant compounds in wastewater. Among AOPs, semiconductor photocatalysis is widely studied because it is an advance, eco-friendly, recyclable, sustainable technology, cost-effective, and the energy consumption is much lower than other advanced oxidation processes, due to solar radiation could be used for photocatalyst activation [30]. This process involves highly reactive intermediates particularly the hydroxyl radical (OH·). Hydroxyl radical is a highly reactive oxidant (Table 1) with oxidation potential 2.8V vs NHE (normal hydrogen electron) after fluorine radical.

$$\text{Organic species} + OH\cdot \rightarrow CO_2 + H_2O + \text{inorganic ions}$$

Table 1: Oxidation potential of different Molecule [31]

Reactive species	Symbol	Oxidation Potential (V)
Fluorine	F_2	3.00
Hydroxyl radical	$OH^{\cdot}$	2.80
Hydrogen peroxide	H_2O_2	1.76
Ozone	O_3	2.07
Hypochlorous acid	HOCl	1.49
Chlorine	Cl_2	1.36
Hypobromous acid	HOBr	1.33
Hypoiodous	HIO	0.99
Chlorine dioxide	CLO_2	0.95
Iodine	I_2	0.54

Oxygen	O_2	0.40

2.3.1. Photocatalytic Dye Degradation

Photocatalysis is one of the rapidly developing advanced oxidation processes (AOP), which absorbs light and initiates a chemical reaction or modifies its rate without itself being involved [32]. The word photocatalysis came from Greek origin and composes of two parts: the prefix-photo (photons: light) and the word-catalysis (katalyo: break apart, decompose). Although there is no consensus in the scientific community as to a proper definition of photocatalysis, the term can be generally used to describe a process in which light is used to activate a substance [33]. Based on the difference in the phase of reacting species and the catalyst, the photocatalytic processes can be categorized as homogeneous and heterogeneous photocatalysis.

In homogeneous photocatalysis, the substrates, and the photocatalysts should be in the same phase. The best commonly used homogeneous photocatalysts include ozone and Photo-Fenton systems. But in the case of heterogeneous photocatalysis, the photocatalysts and the reactants are present in different phases [34]. Heterogeneous photocatalysis uses semiconductors, as a photocatalyst and has an active area for Uv-vis irradiation then catalyst could split/break the substance in various species. This discovery has since been regarded as a stepping-stone for the numerous other studies carried out on photocatalysis to date [35]. This mechanism can be applied to low, biodegradable, high complexity, and high concentration of pollutants in wastewater [36]. A variety of heterogeneous photocatalysts such as metal, metal oxide, semiconductors, carbon-based nanoparticles, quantum dots, and other materials have been studied for dye degradation in wastewater [37]. The light sensitizing ability of semiconductor photocatalysts is due to the electronic structure characterized by the filled valence band which is analogous to the highest occupied molecular orbital (HOMO) and an empty conduction band which is analogous to the lowest unoccupied molecular orbital (LUMO). The valence band and conduction band are separated by an energy gap called the bandgap (Eg) [39].

2.3.2. Principle of Heterogeneous Photocatalysis

The Heterogeneous Photocatalytic process involved the illumination of semiconductor photocatalyst with ultraviolet or visible light irradiation to initiate a redox environment [38]. The bandgap also determines the wavelength sensitivity of the semiconductor to irradiation. The semiconductor photocatalysts absorb a photon with energy equal to or higher than its

bandgap to excite an electron from the valence band to the conduction band to produce negative conduction band electrons and positive valence band holes [40] which is shown in Figure 3

$$\text{Semiconductor} + h\nu \rightarrow e\,(cb)^{-} + h\,(vb)^{+} \qquad \text{eqn (1)}$$

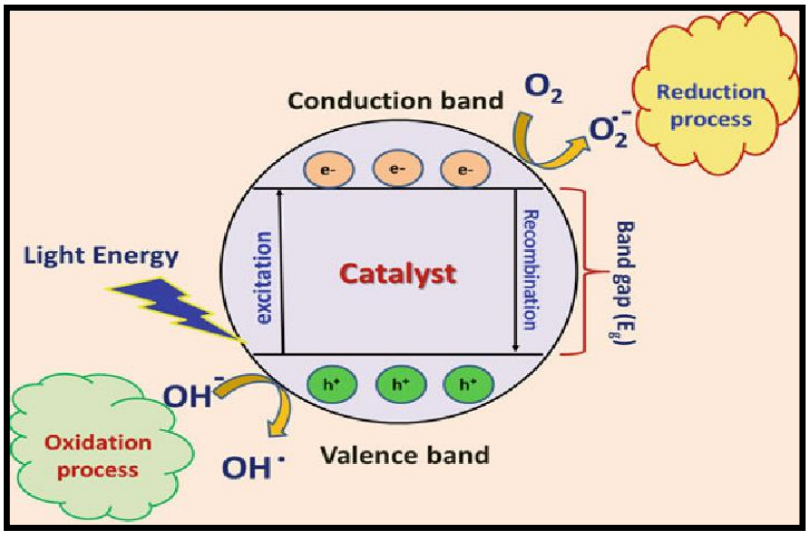

Figure 3: General working principles of the photocatalytic dye degradation mechanism [41]

Subsequently, the generated charge carriers diffuse to the particle surface to participate in the redox reaction with the adsorbed substrate. The holes in the valence band should have a chemical potential of +1.0 to 3.5V versus NHE to induce the oxidation of the adsorbed substrate directly, assuming that the substrate has a redox potential suitable for the thermodynamically allowed reaction [42]. However, most holes react with surface adsorbed water molecules to produce hydroxyl radicals (•OH) which have strong oxidizing power with the oxidation potential of 2.80 V versus NHE [43].

$$h^{+} + H_2O \rightarrow \bullet OH + H^{+} \qquad \text{eqn (2)}$$

Meanwhile, the conduction band electrons are a good reducing agent (0.5 to -1.5V versus NHE) [44], and may also be scavenged by dissolved oxygen to form a superoxide radical ($O_2^{-\bullet}$). The superoxide radical ion can act as both a reducing and oxidizing agent. They are quite stable in aprotic solvent but in an aqueous solution, they react with a proton to form hydrogen peroxide and successively form hydroxyl radicals [45].

$$e^{-} + O_2 \rightarrow O_2^{-\bullet} \qquad \text{eqn (3)}$$

$$O_2^{-\bullet} + H^{+} \rightarrow HO_2^{-\bullet} \qquad \text{eqn (4)}$$

$$HO_2^{-\bullet} + e^{-} + H^{+} \rightarrow H_2O_2 \qquad \text{eqn (5)}$$

$$H_2O_2 + e^{-} \rightarrow \bullet OH + OH^{-} \qquad \text{eqn (6)}$$

2.4. Parameter Affecting the Photocatalytic Activity

There are several parameters on which the oxidation rate and the efficiency of photocatalytic activity highly depend, the effect of pH, initial concentration of dyes, the dosage of catalyst, the intensity of light, Size and surface of the catalyst, and the effect of temperature.

2.4.1. Effect of pH:

Photocatalytic activity is highly dependent on the pH of the solution in which the photocatalyst is dispersed. The variation of pH changes the charge of the catalyst particle, size of aggregates, the position of conductance and valence bands, and shifts the potential of catalytic reaction. By varying the solution pH, the adsorption of the pollutants on the catalyst surface can be changed. For example, for titanium in an acidic solution, the surface becomes positive while in alkaline media it will become negatively charged. Therefore, it is favorable the adsorption of dye under acidic solution because of hydroxyl ion. Generally, the particle surface will remain positively charged in the acidic medium and negatively charged in the basic medium [46,47].

2.4.2. Effect of Initial Dye Concentration:

This is also one parameter that needed to be taken into account. Generally, as the initial concentration of dye increases, there is a decrease in photocatalytic activity. Because the reason that when the dye concentration increase it is difficult for photons to reach the catalyst surface so there is less formation of hydroxyl ion which affects the degradation The rate of photocatalysis also changes depending on the chemical nature of the pollutant [47].

2.4.3. Effect of Photocatalyst Concentration:

Effect of photocatalyst concentration, which has a great influence on the Photocatalysis activity**.** The concentration of catalyst affects the overall photocatalysis reaction rate, where the dosage of catalyst is directly proportional to the overall photocatalytic reaction in heterogeneous catalytic activity because when we increase the number of catalysts the number of the active site on the surface of the photocatalyst also increase which makes the increase in the formation of OH^* radicals. However, when the dosage of catalyst is above saturation stage, the light photon absorption coefficient decreases and the excess photocatalyst can create a light screening effect that decreases the surface area exposed to irradiation and the solution become turbid which then blocks UV- radiation that reduces the efficiency of the photocatalytic process [48].

2.4.4. Effect of size and surface of the catalyst:

In photocatalytic degradation, process surface morphology such as particle size and agglomerate size is one parameter that needs to be considered because there is a direct relationship between organic compounds and surface coverage of the photocatalyst. The reaction takes place only in the absorbed phase of the photocatalyst as photons strike the photocatalyst surface. It shows, Nanoparticle has a higher degradation rate because they have higher surface area than the bulk materials [49].

2.4.5. Effect of Temperature:

This is also an important parameter, which is needed to be considered. Generally, when the reaction temperature increase there is also an increase in photocatalytic reaction. However, reaction temperature above the optimum degree promotes the recombination of the charge carriers and disfavors the adsorption of the organic compound on the catalyst surface. A reaction temperature below 0°C results in an increase in the apparent activation energy [50]. As we, increase the temperature there was a formation of a bubble in the solution, which causes the formation of free radicals. so as we increase the temperature which may increase the oxidation rate of dye at the interface [51].

2.4.6. Light Intensity:

Light intensity is also one parameter that affects the degree of photocatalytic reaction. To get a high photocatalytic reaction rate, high light intensity is required to adequately provide each of the photocatalysts' surfaces active sites with sufficient photons energy required [52,53].

2.5. Semiconductor Photocatalysts

Semiconductors are solids characterized by intermediate electronic behavior, and their resistance (or conductivity) is between the dielectric and the conductor [54]. The electronic structure of a solid can be well explained using bandgap theory. According to this theory, two bands for a crystalline solid are proposed namely, the valence band (VB), which is the highest occupied molecular orbital (HOMO) comprising of bonding orbital, and the conduction band (CB), which is the lowest unoccupied molecular orbital (LUMO), comprising of anti-bonding orbitals. The two bands are detached by a prohibited zone known as the bandgap or energy gap (Eg). In the case of metallic conductors, there is superficially an absence of a bandgap between the VB and the CB due to the overlapping of the molecular orbital. Whereas, insulators have a large bandgap that separates the VB and the CB. A relatively intermediate bandgap is present

between the VB and the CB in the case of semiconductors [55]. In recent years, semiconductor chalcogenides have received more and more attention and have been applied as photocatalysts because of their physical, chemical, magnetic, surface electronic, optical properties, charge transport characteristics, excited-state lifetime, and due to their small size than Bulk materials [56, 57]. Chalcogenides metal oxides such as TiO_2 Chalcogenides metal oxides such as TiO_2 [58, 59], ZnO [60, 61], WO_3 [62], SnO [63, 64], ZnS [65, 66], PbS [67, 68], SnS [69], CuS [70, 71] and CuSe [72] are commonly used as photocatalyst semiconducting materials. Many synthetic methods have been developed to produce semiconductor nanoparticles with controlled physical and chemical properties [73].

Among the copper chalcogenides, CuSe is typical p-type semiconductors, which have potential applications in super capacitors [74], Li-ion batteries [75], solar cells [76, 77] gas sensors [78], medical devices [79, 80], and photo-catalysts [81, 82] due to their good physical, chemical, electrical, biochemical and optical properties. Since the outstanding properties have a direct correlation with their micro-morphologies [83].

2.5.1 Copper Selenide

Copper selenide is a *p-type* semiconductor with a direct bandgap, as well as an indirect bandgap [84]. The stoichiometric and phases of copper selenide are more than another metallic selenide This is because copper exists in more than one oxidation state such as +1, +2, +3, and + 4. Different stoichiometric (CuSe, Cu_2Se, Cu_2Sex, $CuSe_2$, Cu_3Se_2, Cu_5Se_4 and Cu_7Se_4) and nonstoichiometric ($Cu_{2-x}Se$) compositions and structural forms of copper selenide are well-documented [85].

The crystal structure of klomannite copper selenide (CuSe)

Depending on the stichometry and the growth method different crystalline phases are occurred such as orthorhombic, cubic, hexagonal, and tetragonal structures [86]. Klomannite CuSe has a hexagonal crystal structure with a space group of D_{6k}^4-$p6_3/mmc$**.** Has a= 3.938 c= 17.25A^0 and cell content six with two Cu1 atoms on 2(d) Wyckoff sites (1/3, 2/3, 3/4), four Cu2 atoms on 4(f) sites (1/3, 2/3, Cuz), two Se1 atoms on 2(c) sites (1/3, 2/3, 1/4) and four Se2 atoms on 4(e) sites (0, 0, Sez). Cu1 atoms are coordinated to three Se1 atoms in the (0001) plane, while Cu2 is surrounded by three Se2 atoms and one Se1 atom in a nearly perfect tetrahedral coordination [2, 87]. CuSe has a hexagonal crystal structure with trigonal planar CuX_3 units surrounded by tetrahedral CuX4 units (CuX_4- CuX_3-CuX_4), which are held together by

covalent bonding between X atoms from each layer. And this CuSe has a hexagonal super structure of 13 [88].

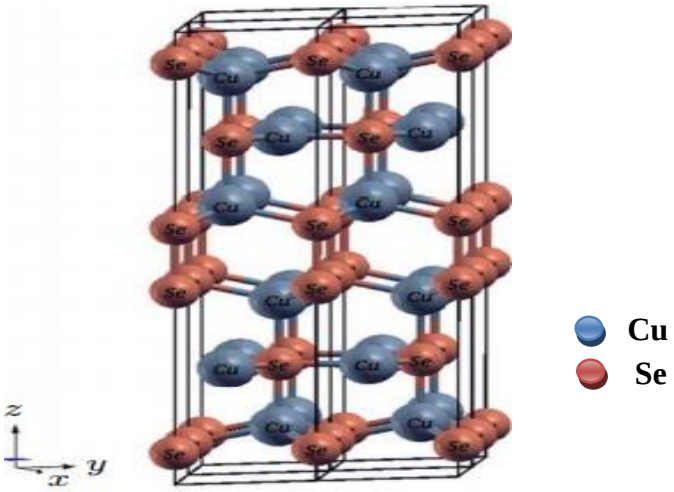

Figure 4: Klomannite copper selenide (CuSe) [1, 2]

For the synthesis of copper selenide different methods are developed such as hydrothermal method [81, 89], chemical vapor deposition method [85, 90], solvothermal method [91, 92], son chemical method [93, 94], and co-precipitation method [89, 93, 95, 96]. Among them, this paper uses the hydrothermal synthesis method. Hydrothermal synthesis usually refers to heterogeneous reaction or chemical reaction between substances in aqueous media above 100°C and one bar with good crystallites as well as high efficiency. This method is used for the preparation of super-ionic conductors, chemical sensors, magnetic materials, and luminescence phosphors [97, 98].

Previously several techniques have been made to degrade organic dyes, such as adsorption, oxidation, and biological treatment. However, those methods have a few disadvantages, for instance, biological treatment requires a calm environment to achieve proper removal of pollutants, but its biodegradation rate is slow. In the case of adsorption, it can remove pollutants effectively, but it may generate secondary pollution during the regeneration and desorption process of saturated adsorbent [100].

New photocatalytic cloth supplying excessive performance has been advanced for greater photocatalytic overall performance on wastewater contaminants. Heterogeneous photocatalyst has become a broadly used approach for various applications of renewable energy, organic synthesis, and environmental pollutants treatment. This approach is most effective because of

its advantage, including being recyclable, easy catalyst separation, and tunable active sites using morphology and porosity [54]. There are different fabrication techniques such as sol-gel, surface coating, hydrothermal, solvent casting, surface modification, three-dimensional printing, and low temperature ultrasonic are used [101]. Among; various photocatalysts, metal selenide has been studied because they show important electrical, optical, and electrical properties due to absorption of light in the visible region and transferred electrons to large bandgap semiconductors. CuSe is one of the members of the first-row transition metal chalcogenides with different phase, stoichiometric and non-stoichiometric forms [102]. Copper selenide is a p-type semiconductor used for different applications such as solar cells, superionic conductors, optical filters, cancer therapy, and optoelectronic devices [103].

Previously many researcher groups have reported about copper selenide among these the hydrothermal synthesis method for the hexagonal CuSe nanoflakes. For the formation of hexagonal CuSe nanoflakes, the concentration of NaOH and polyvinylpyrrolidone has a great impact. The Photocatalytic activity of the hexagonal copper selenide nanoflakes has also been studied for the degradation of organic methylene blue under sunlight irradiation. After sunlight irradiation at about 99% of the MB, degrade in 25 minutes. Dendrites' CuSe with hierarchical side branches was also synthesized by rapid, one-pot, facile, green hydrothermal route. In dendrite copper selenide, kiwi juice is used as a reducing and coating reagent. The thin films in the copper selenide nanoparticle. High-quality thin film with desired property can be achieved photocatalytic activity of the dendrite CuSe has been studied by photocatalytic degradation of malachite green under sunlight light irradiation. Above 97%, MG in wastewater can be degraded in 30 minutes after sunlight irradiation because of their side branched structure, which helps for the strong adsorption of MG. The photocatalytic activity performs excellent degradation by combining highly efficient adsorption and natural daylight-driven photocatalysis [81, 104]. The photocatalytic activity performance of copper selenide nanostructure is strongly dependent on the molar ratio of Se/Cu [0.16 – 1.5]. When Se/Cu >1 the mixture of nanoparticles with spherical and Nano disc with a hexagonal shape were obtained and for Se/Cu < 1 particle-like structure is obtained. When the ratio of Se/Cu changes different phases such as $Cu_{1.8}Se$, CuSe and Cu_3Se_2 were formed. The degradation efficiency to degrade methylene blue (MB) and malachite (MG) is higher when the Se/Cu ratio is greater than one and the optimum ratio for Se/Cu is 1.4 to get the highest photocatalytic activity performance [89]. Photocatalytic activity is also highly dependent on the pH of the solution. Because pH has an effect on the size and shape of nanoparticles and the configuration by the role of pH. As pH increase, the growth of particles in the copper selenide, thin films also

increase which, forms bigger particle. In this report, the optimum concentration of pH is 10 for good photocatalytic performance. The photocatalytic activity of copper selenide has also been studied. About 91% of methylene blue and Congo red organic pollutants are degraded under visible light [105]. CuSe nanoparticle and CuSe quantum dot are synthesized by the reflux condensation method. The optical absorption of both is studied under different reaction temperatures (50°C, 70°C, 90°C) and for different reaction times (4hr, 8hr, 12hr). The CuSe has a maximum absorption band at 350 nm at 50°C for 12hr, and at 70°C, the absorption band becomes stronger and sharper with 345 nm wavelength, and when temperature increase to 90°C the absorption band shifted towards a shorter wavelength 344 nm. In addition, the quantum dot CuSe has a maximum absorption band at 383 nm for 50°C for 12hr. At 70°C, the absorption band becomes stronger and sharper with a 371 nm wavelength. As the temperature increase to 90°C, the absorption band shifted towards a shorter wavelength of 360 nm. Generally, when temperature increases the size of a particle decrease, which cause the surface-to-volume ratio to increase. The photodegradation was examined for two organic dyes methylene blue (MB) and Rhodamine-B (RhB) for CuSe nanoparticle at 90°C for 12 hours. The degradation efficiency for RhB and MB are calculated 87 and 76% respectively when 3mg of CuSe dissolved in l mol aqueous solution of RhB and MB. And also the degradation efficiency of the CuSe quantum dot was evaluated by decomposition of Rhodamine-B and the performance for the CuSe quantum dot is calculated 70% when 0.003gm of CuSe was dispersed in 1 mol of an aqueous solution of RhB [85, 106]. Reaction temperature has also a great effect on the structure, composition, and morphology of copper selenide nanocrystals. As the temperature increases the Cu: Se ratio in α-copper selenide also increases. As the reaction temperature increase, different phases results such as $Cu_{1.8}$ Se, Cu_2Se, and $Cu_{2.5}Se$ nanocrystals at20°C, 23°C, and 260°C, respectively. There is also a transfer of crystals from the α-phase to the β-phase because of silver doping. This report also showed that the optical and photo electrochemical properties of copper selenide that battery electrodes can be self-repaired when they are exposed to sunlight [107].

Doping is one of the most important techniques for reducing the gap between photocatalysts. The narrowing allows the photocatalyst to be active in visible light, thereby enhancing its quantum efficiency and electronic structure kinetics to improve the performance of CuSe in photocatalysis. A concentrated alkaline hydrothermal method is also used for the synthesis of sulfur-doped copper selenide hexagonal nanoflakes. They studied the effect of NaOH concentration, reaction temperature, and surfactant and Cu source on the morphology of as-synthesized $CuSe_{1-x}S_x$ nanoflakes. As x (0.1-0.5) the band gaps are tunable which can easily

be realized by changing the ratio of Se/S in the mixture. The photocatalytic degradation efficiency of $CuSe_{1-x}S_x$ is also studied for organic dye methylene blue (MB) in the presence of H_2O_2 under visible light irradiation, the report showed excellent photocatalytic activities of hexagonal $CuSe_{1-x}S_x$ nanoflakes [108].

For enhanced photocatalytic activity different methods are, using one of them is making a composite with the photocatalysts. Reports showed that composite-based CuSe nanostructure was developed last few years; this composite has an advantage because it reduces the recombination rate of the photo regenerated charge carrier to enhance the performance of the photocatalytic activity. Most dyes are synthetic, including anionic such as acid, reactive, direct, cationic, and non-ionic dyes. According to chemical structure, they are divided into azo, anthraquinone, indigoid, nitroso, and nitro dyes. Dyes are frequently used in many industries such as textile, leather, paper, rubber, printing, plastics and they are chemically stable and resistant to degradation after removing as waste in the water. This remaining in water for a long time causes a huge risk to the environment because dyes can reduce sunlight transmission and contain toxic substances, such as heavy metals including lead, chromium, and aromatic compound.

Composite of CuSe nanoparticle and graphene oxide (CuSe/GO) was designed by hydrothermal route. To evaluate the photocatalytic activity, the CuSe and CuSe/GO were used to degrade methylene green dye. To get the enhanced dye to remove the parameter like initial methylene concentration, pH of the solution, dose of the catalyst, and contact time were optimized. The MG was conducted in a control experiment such as dye/sunlight and dye/H_2O_2 for both CuSe and CuSe/GO composite. The performance were investigated in pH (2 to 8), does of catalyst (0.005-0.07g/mL), initial dye concentration (20-40mg/L) and irradiation time (15-150min).The optical properties showed that CuSe nanoparticle has a maximum absorbance around 400nm with a 3.1ev band gap value, and the CuSe/GO composite has maximum absorbance compared with CuSe nanoparticle which is around 460 nm having a bandgap of 2.7ev which indicate the band gap was reduced in the composite which is important for the absorption of visible light for improving the performance of degradation. When we compare the efficiency for the degradation of MG dye, the CuSe and CuSe/GO composite have dye degradation at about 81 and 89% within 60 and 45 minutes under sunlight irradiation, respectively [109].

A simple, low-cost with two-electrode electrochemical technique and the photocatalytic prepared $Cu_{2-x}Se$ thin film with cubic berzelianite phase and thermoelectric properties of the

thin films were investigated results showed that $Cu_{2-x}Se$ crystallized in the cubic phase of Berzelianite and was found to have direct and indirect bandgaps of 2.9 and 1.05 eV respectively, covering almost the entire range of the solar spectrum**.** Photocatalytic decoloration of aqueous methylene blue (MB) and bengal pink (RB) dyes on Cu2-XSe thin films was investigated under visible light irradiation. Cu_{2}-$_{X}Se$ thin films showed higher MB catalytic activity than RB in the presence of H_2O_2. The photocatalytic discoloration followed first-order reaction kinetics. Complete removal of aqueous MB was realized after visible light irradiation for 150 min with $Cu_{2-X}Se$ thin film catalyst in presence of H_2O_2. Thermoelectric performance was evaluated through the power factor and figure of merit. The concentration of carriers obtained from thermoelectric energy was used to assess the mobility of carriers by measuring electrical conductivity [110].

The present study successfully fabricated $Cu_{2x}Se$ / rGO heterojunctions for the first time using hot in situ injection methods and used them to produce photocatalytic hydrogen. h, almost 3.46 times higher than that of pure $Cu_{2x}Se$. The increased activity can be attributed to facilitated light absorption, upregulated charge density, lower interfacial transfer resistance, and longer electron decay time. During this time, the enlarged specific surface can create more active reaction sites, leading to the improvement of the photocatalytic properties. In addition, the mechanism of hydrogen production of the $Cu_{2x}Se$ / rGO heterojunction is proposed [110]

Copper selenide (CuSe) nanoplates have been hydrothermally synthesized from copper sulfate as the source of copper and selenium powder as the source of selenium. Disodium EDTA (EDTA) has been used as a surfactant to moderate the surface morphology of copper selenide nanoparticles. shows the influence of different concentrations of EDTA on the morphology of copper selenide nanoplates. These CuSe nanoplates have been characterized by X-ray diffraction (XRD), X-ray energy dispersal spectroscope (EDS), scanning electron microscope (SEM) and Raman spectrometer, UV-visible spectroscopy (Uv-vis), and photoluminescence (PL)[111].

Moreover, some groups studied that the rectifying behavior and photocatalytic activity in ZnO nanorods array /Ag/CuSe hetrostructure. These ternary ZnO nanorods/Ag/CuSe hetrostructure are fabricated by solution route, thermal evaporation, and magneto sputtering process. Rhodamine B was the organic dye in which the photocatalytic performance was estimated. The ternary ZnO nanorods/Ag/CuSe hetrostructure has higher photocatalytic efficiency than ZnO NRS/CuSe due to the three functional components coupling [112].

CuSe-PDA/g-C_3N_4 composite is also used for the degradation of dyes. CuSe and PDA were prepared by the liquid phase co-precipitation method and the CuSe-PDA/gC_3N_4 composite was prepared by the hydrothermal method. This group is studied the photocatalytic performance of CuSePDA / gC_3N_4 by adding polydopamine carbon nitride (PDA) in the graphite phase (gC_3N_4) was better than CuSe and PDA. Methylene blue was the organic dye in which photocatalytic performance was estimated and it was optimized that approximately 99% of 50 mg / L MB was degraded within 60 minutes of irradiation [113].

CHAPTER THREE

3. Methodology

3.1. Materials

For this work, analytical grade chemicals such as copper chloride dehydrate ($CuCl_2.2H_2O$) (99.5%), selenium powder (Se) (99.5%), thiourea (CH_4N_2S) (>98.5%), sodium hydroxide (NaOH) (99%), cetyltrimethylammonium bromide (CTAB) (>98%), methylene blue ($C_6H_{18}C1N_3S.3H_2O$), distilled water, and ethanol were used. The entire chemicals used for the experiment were purchased from Blulux laboratories, Lab tec chemicals, Loba Chemie Pvt. Ltd., India, and Finkem laboratory reagent. All other reagents were of analytical grade and were used without further purification. All the solutions were prepared using distilled water.

3.2. Methods

This study uses the hydrothermal synthesis method. Hydrothermal synthesis usually refers to heterogeneous reaction or chemical reaction between substances in aqueous media above 100°C and one bar with good crystallites and high efficiency. This method is used to prepare superionic conductors, chemical sensors, magnetic materials, and luminescence phosphors. [31]. Sulfur doped copper selenide is synthesized with this method because this method is important for controlling the morphology of the material to be prepared and also generates nanomaterials that are not stable at high temperatures. [114].

3.2.1 Synthesis of sulfur-doped copper selenide photocatalyst ($CuSe_{1-x}S_x$)

The Cu (Se, S) was synthesized using a simple hydrothermal method, as shown in Figure 5. A typical preparation process for Cu (Se, S) was carried out: 0.0149 moles of $CuCl_2.2H_2O$ and 0.0011 moles of CTAB were dissolved in sodium hydroxide solution (10 M) then the mixture was stirred for 60 minutes with magnetic stirring. After that 0.025 moles of Se powder and $5*10^{-4}$ moles of CH_4N_2S were added to the mixture and stirred for another 60 minutes to ensure good dispersion of the reactants. Then the final solution was transferred into a Teflon-lined stainless-steel autoclave, maintained for 130 ℃ for 4 hours, and then cooled down to room temperature naturally. Finally, the final black precipitate was washed with distilled water several times and with ethanol twice and dried in an oven at 80 ℃.

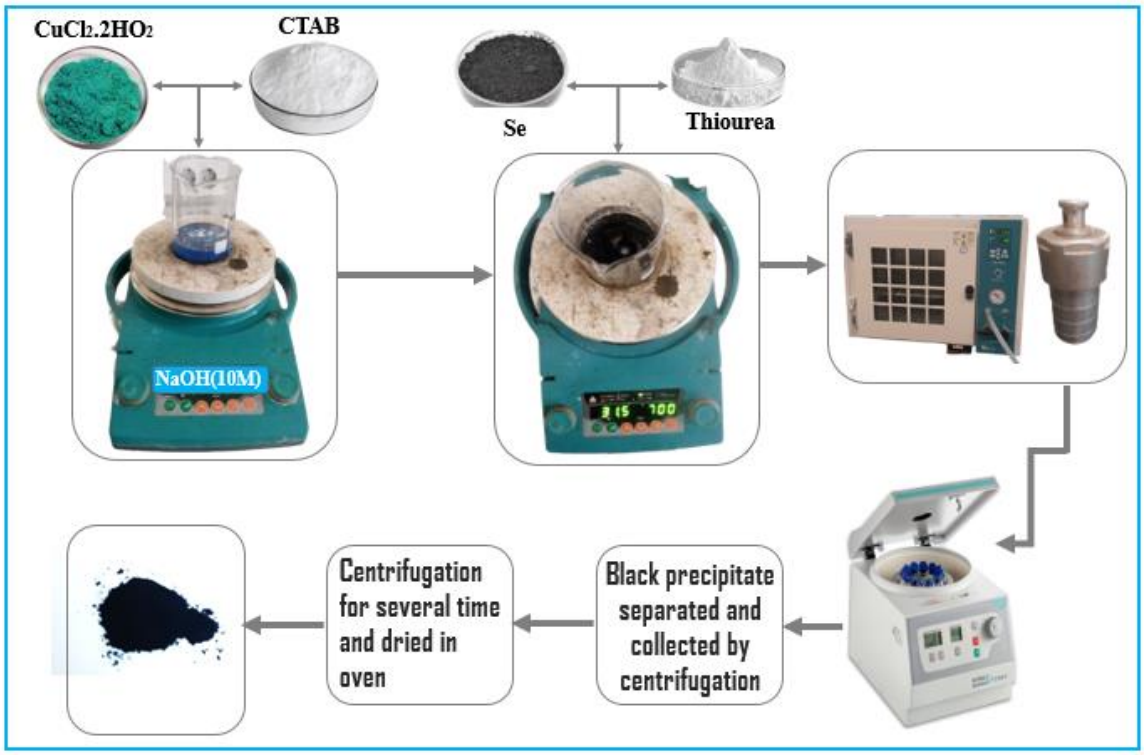

Figure 5: Preparation of sulfur-doped copper selenide photocatalyst ($CuSe_{1-x}S_x$)

3.3. Instrumentation

3.3.1 X-Ray Diffraction (XRD)

X-ray diffraction study of the prepared catalysts was carried out using an X' per PRO diffractometer with the following conditions: λ Cu Kα = 0.15406 nm, 40 kV, and 30 mA, in the 20 to 80° (2θ) region. Data were collected with a counting rate of 1°C/min. The average crystallite size of the prepared catalysts was estimated using the Scherer equation (Eq.3.1).

$$P = 0.94\,\lambda / \beta \cos\theta \qquad \text{Eq (3.1) [115].}$$

Where, P - Crystallite size, λ - Wavelength (1.54A°), β - Full width at a half-maximum height of the XRD peak, and θ - Diffraction angle

3.3.2 UV-Vis Diffuse Reflectance Spectroscopy

Band-gap energies of all the prepared catalysts were evaluated by UV-Vis-DRS spectra. Diffuse reflectance spectrophotometer (Shimadzu UV-2450) equipped with an attached integrating sphere. The spectral data were acquired in the 200 to 800 nm range, with 0.5 nm data pitch and 100 nm/min scan speed and $BaSO_4$ as a reflectance standard. The original

coordinates of the spectra (reflectance vs wavelength) were transformed to Kubelka–Munk function (K) vs photon energy (hν). The band-gap energy of the prepared catalysts was calculated using the following equation $(\alpha h\nu)^{n} = k\,(h\nu - Eg)$ where α is the absorption coefficient of the prepared catalysts, Eg is band-gap energy, k is a constant involving properties of the bands, hν is the photon energy and n is 1/2, 3/2, 2, and 3 for directly allowed, directly forbidden, indirectly allowed, and indirectly forbidden transitions, respectively [116, 117].

3.3.3 Scanning Electron Microscopy (SEM)

The structural morphologies of the samples were also examined by scanning electron microscopy (SEM) model COXIEM-30.

3.3.4 Photoluminescence spectroscopy (PL)

Photoluminescence (PL) spectroscopy measures the radiation emitted by a material after excitation. PL spectroscopy is a non-destructive technique for the characterization of various organic and inorganic materials including semiconductors and the investigation of their electronic structure. It is also helpful in determining material imperfections and impurity concentrations. PL spectroscopy also shows application to microscopic imaging of biological molecules. Photoluminescence spectra of the samples were recorded on PL (VIRAN-CARY ECLIPSE) device with λ_{exc} = 357nm.

3.3.5 Fourier Transform-Infra Red Spectroscopy (FTIR)

FT-IR spectroscopy is used for the identification of the functional groups present in all the prepared catalysts. The prepared catalysts were mixed with spectroscopic grade KBr and made into pellets. FT-IR spectra were recorded using a Perkin Elmer 6X spectrometer with a frequency range from 4000 to 400 cm^{-1}.

3.4. Photocatalytic Experiments

The photocatalytic degradation of MB dye was carried out using the prepared catalyst dispersed in the aqueous solution of the dye in a cylindrical-shaped photocatalytic quartz reactor as in Figure 6. For this work, 10 ppm MB standard solution was used. In a typical experiment, a 0.05g of photocatalyst is mixed in 100 mL MB aqueous solution. Then the solution was stirred for 30 min in the dark to obtain the adsorption-desorption equilibrium for the dye. After that, the solution was exposed to 150 W light source visible light. After a

specific time, interval, 5 mL aliquots were withdrawn and centrifuged at 5000 rpm for 15 min to separate the photocatalyst powder and analyzed using a UV-visible spectrophotometer to obtain the concentrations of MB at various time intervals. The photocatalytic experiments for the temperature study were conducted by heating the mixture with a resistance heater and a thermocouple being used to measure the mixture and control the system temperature. The dye concentration was determined from the adsorption band at a maximum wavelength of 664 nm.

The degradation efficiency was calculated using the equation below:

$$\text{Efficiency (\%)} = \left(1 - \frac{\text{At}}{\text{A}_\text{o}}\right) \times 100 \qquad \text{Eqn 3.2 [115]}$$

Where A_0 represents the initial concentration of the dye present in the solution and A_t denotes the concentration at any time 't' after irradiation.

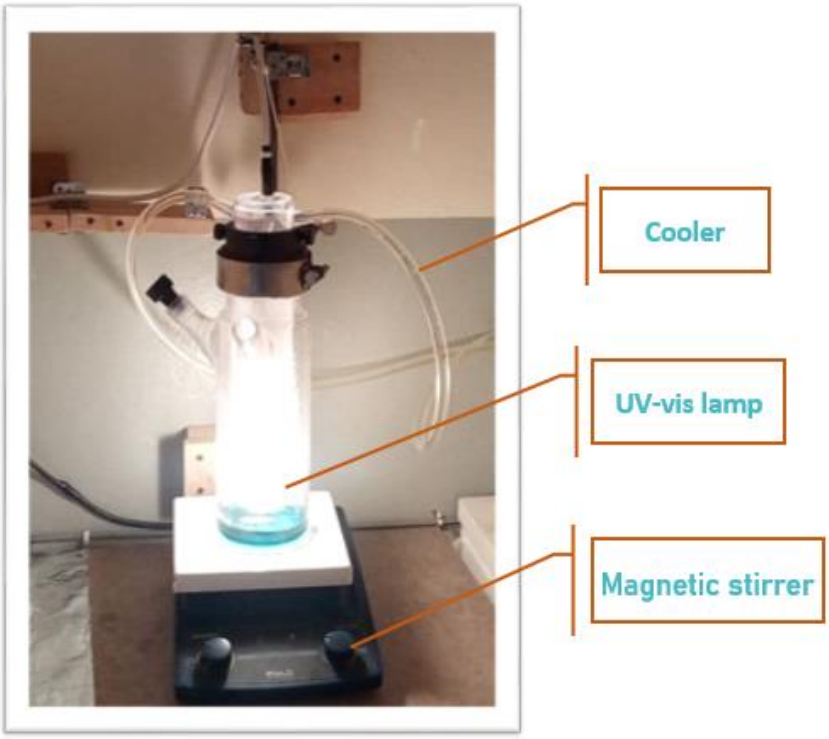

Figure 6: A cylindrical shaped photocatalytic quartz reactor

CHAPTER FOUR

4. Results and Discussions

4.1. XRD Characterization

The phase purity of pristine CuSe and sulfur-doped copper selenide samples with different Sulfur concentrations were examined by XRD as shown in **Figure 7**. The crystal structure of CuSe is klomannite hexagonal crystal structure with a space group of D_{6k}^4-p6_3/mmc and lattice parameter a=3.938A^o c=17.25A^o, this value matches precisely with the standard date (JCPDS card No 34-0171) [118]. One can see clearly that the sharp diffraction peaks at 26.56°, 28.05°, 31.11°, 41.01°, 46.01°, 50.02°, 56.55°, and 70.29° can be assigned to (101), (102), (006), (106), (110), (108), (116) and (208) planes of CuSe respectively. The sharp and strong peak indicates that the formation of CuSe was fully crystallized. The strongest intensity standard diffraction peak indicates that a dominant crystal growth process along the plane (102) [119]. No secondary peaks corresponding to sulfur or any impurity in the XRD pattern were observed. This indicates that the dopant sulfur ion does not significantly affect the crystalline structure of pristine CuSe and the sulfur ions appear to have been successfully substituted into CuSe lattice sites.

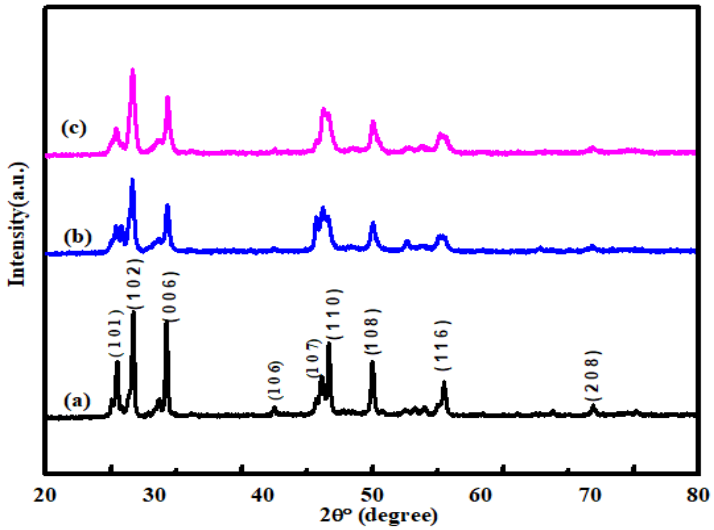

Figure 7: XRD pattern of (a) CuSe, (b) 3% S CuSe, and (c) 5% S CuSe

It can be seen that the diffraction peaks are very similar for CuSe and $CuSe_{1-x}S_x$ with different x values, which is also extremely close compared with the standard pattern of CuSe (JCPDS No.34-0171). According to **Figure 8,** the intensity of copper selenide peaks was reduced in the

doped sample. This indicates the inclusion or insertion of sulfur with layered structures. And also in **Figure 8,** it is observed that the diffraction peaks of copper selenide slightly shift to the higher angle region with increase sulfur concentration, which hints that the doping sulfur ion leads to the reduction of the unit cell. This result is agreeing with the fact that sulfur has a smaller ionic radius (1.02A^{o}) than that selenium (1.16A^{o}). It suggests that the doping sulfur replaces selenium ion [120]. The full width at half maximum (FWHM) of the peaks is enlarged by doping Sulfur. In addition, the full width at half maximum (FWHM) of the peaks is enlarged by the increase of the S concentration that is a sign of a decrease in crystallite size. Therefore, the XRD results indicate that S ions substituted Se ions, successfully.

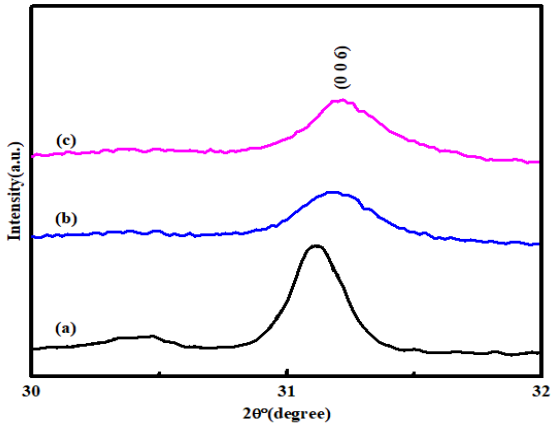

Figure 8: Angle shift due to doping (a) CuSe, (b) 3% S CuSe, and (c) 5% S CuSe

The average crystalline size of the particles was calculated using Debye–Scherer equation:

$$L = 0.9\lambda / \beta \cos\theta \qquad \text{eqn (4)}$$

Where L is the crystallite size, λ is the wavelength of X-rays used for analysis, β is the full width at half maxima (FWHM) of peaks and θ is the diffraction angle.

Table 2: XRD data of CuSe and $CuSe_{1-x}S_x$ synthesized at a different sulfur concentration

Sample designation	**2θ value (deg)**	**FWHM ICSD**	**Crystalline size D XRD (nm)**
CuSe	31.11	0.298	24.8 nm
$CuSe_{0.97}S_{0.03}$	31.18	0.503	13 nm
$CuSe_{0.95}S_{0.05}$	31.22	0.549	9.2 nm

4.2. Fourier Transforms Infrared (FT-IR) Analysis

FT-IR analysis was carried out to identify surface chemistry and bonding vibration of materials [121]. The FT-IR spectra for pure copper selenide and sulfur-doped CuSe are shown in **Figure 9**, in the range, 400-4000cm^{-1} of KBr pressed pellets. From this Figure, it is clear that bands appeared at about 3229cm^{-1}, 3231cm^{-1}, 3216cm^{-1}, bands were stronger than those of usual N-H vibration this may be due to the superimposed N–H vibration with the OH vibrations, corresponding to the adsorption of water on the surface of the sample. The adsorption of water is very common in powder samples with a high surface area that had been exposed to the atmosphere [122]. The band appeared at about 1071 cm^{-1} was assigned to the C–N stretching vibration [123]. The absorption peaks at about 1258 cm^{-1}, 1273 cm^{-1} corresponding to the C–H stretching and bending vibration respectively. The peaks at 428cm^{-1}are related to Cu=Se [124]. The peaks Cu–S is not seen clearly, which might be due to the low doping of S into CuSe lattice. The effect of S doping on the vibration modes of the product was studied, peaks between 400cm^{-1}-1500 cm^{-1} were improved by S-doping. Therefore, the FT-IR results show that S ions have different behavior in the CuSe structure than Se ions. It could be due to the different chemical bond lengths of Cu-Se and Cu-S. In addition, the ionic radius of the S ion is different from that of the Se ion, which results in a difference which leads to modify the intensity of the modes of vibration.

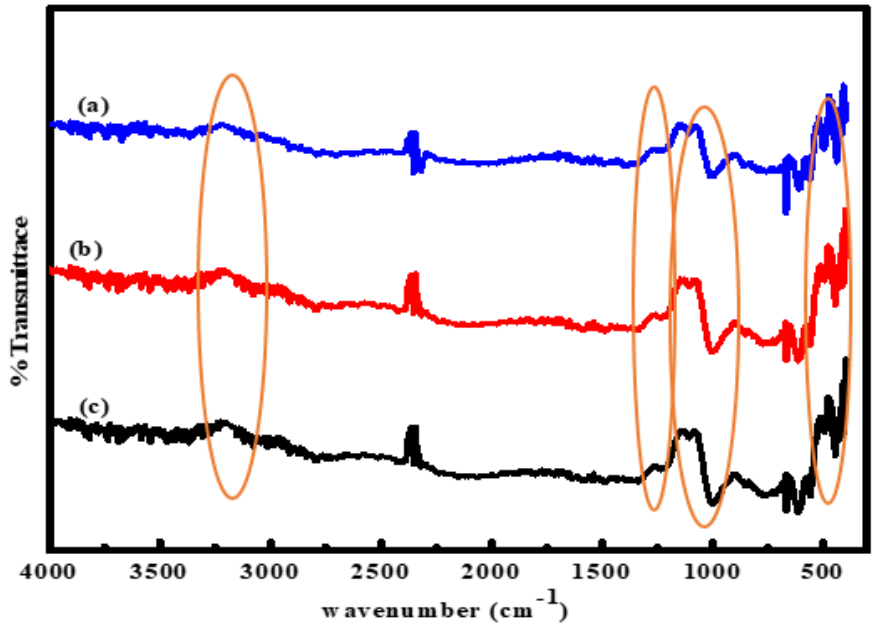

Figure 9: FT-IR spectra of the synthesized (a) CuSe, (b) 3% S doped CuSe, and (c) 5% S CuSe

4.3. Morphological Analysis

The surface morphology (SEM) images of as-synthesized CuSe, $CuSe_{1-x}S_x$ samples are shown in **Figure 10(a)-10(c).** The pristine CuSe has almost the like morphology as that of sulfur-doped copper selenide $CuSe_{1-x}S_x$. The SEM micrographs reveal that it is possible to make the morphology remains the same when using S atoms to replace segmental Se atoms in CuSe. We can attribute this observation to the fact that $CuSe_{1-x}S_x$ have the same morphology and only a slight difference exists between S and Se atoms in their atomic radius [81]. In **Fig 10 (d),** it is observed that several crystallites come together to form grains and that non-uniform and undefined boundaries of different sizes are also observed. In **Figure 10(e),** it can be seen that the synthesized pristine CuSe with smooth surface and relatively symmetrical hexagonal shapes [81, 108].

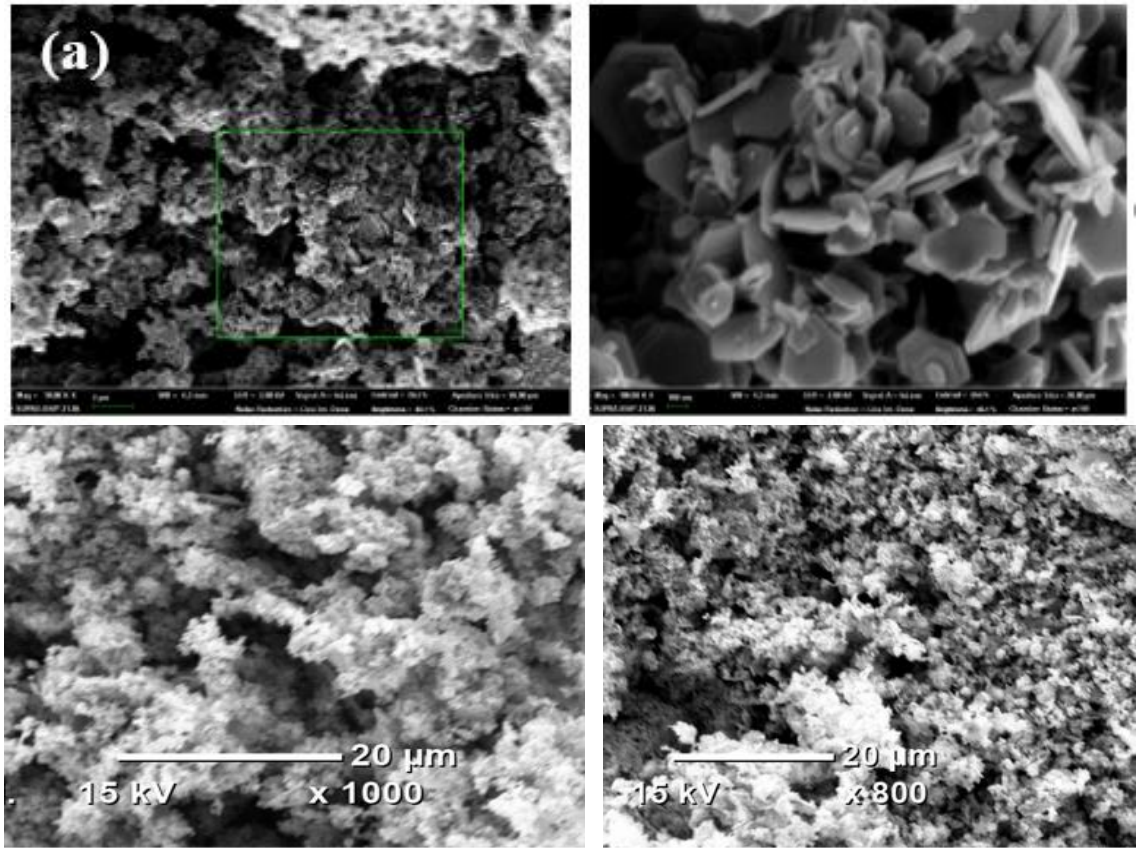

Figure 10 : SEM image of (a) CuSe, (b) 3% S CuSe, and (c) 5% S CuSe (d) CuSe FSEM (e) CuSe

4.4. Diffuse Reflectance Spectroscopy

The absorption spectra of CuSe and $CuSe_{1-x}S_x$ with different x values are shown in **Figure 11** The direct bandgap energies of the products can be estimated from a graph of (αhυ) 2 as a function of the photon energy (hυ) according to the Kubelka-Munk model, where is the absorption coefficient, Eg is the bandgap energy, k is a constant involving the properties of the bands, hν is the energy of the photon and n is respectively 1/2, 3/2, 2 and 3 for directly authorized, directly forbidden transitions, indirectly authorized and indirectly prohibited [125]. According to this plot, the bandgap of pristine copper selenide is almost similar to that of sulfur-doped copper selenide. A broad-spectrum response in the wavelength range of 400- 800 nm is plotted in the absorption spectra of the $CuSe_{1-x}S_x$. For x= 0, 0.3, and 0.5, the Eg is about 2.33, 2.3 and 2.32 respectively. The outcomes are similar to the previous report and therefore suitable for photoelectric applications [108]. The bandgap result indicates that the difference between the Eg of CuSe and CuS is quite small. That is why the values of Eg for $CuSe1-_xS_x$ (x= 0.3, and 0.5) and CuSe are numerically close. In addition, these relative Eg values also reveal that the optical properties of as-synthesized $CuSe_{1-x}S_x$ are very close, though the values of x (x=0, 0.3, and 0.5) are different. Moreover, the value of Eg of $CuSe_{1-x}S_x$ also decreases slightly, with the value of x increasing from 0.3 and increase for x=0.5.

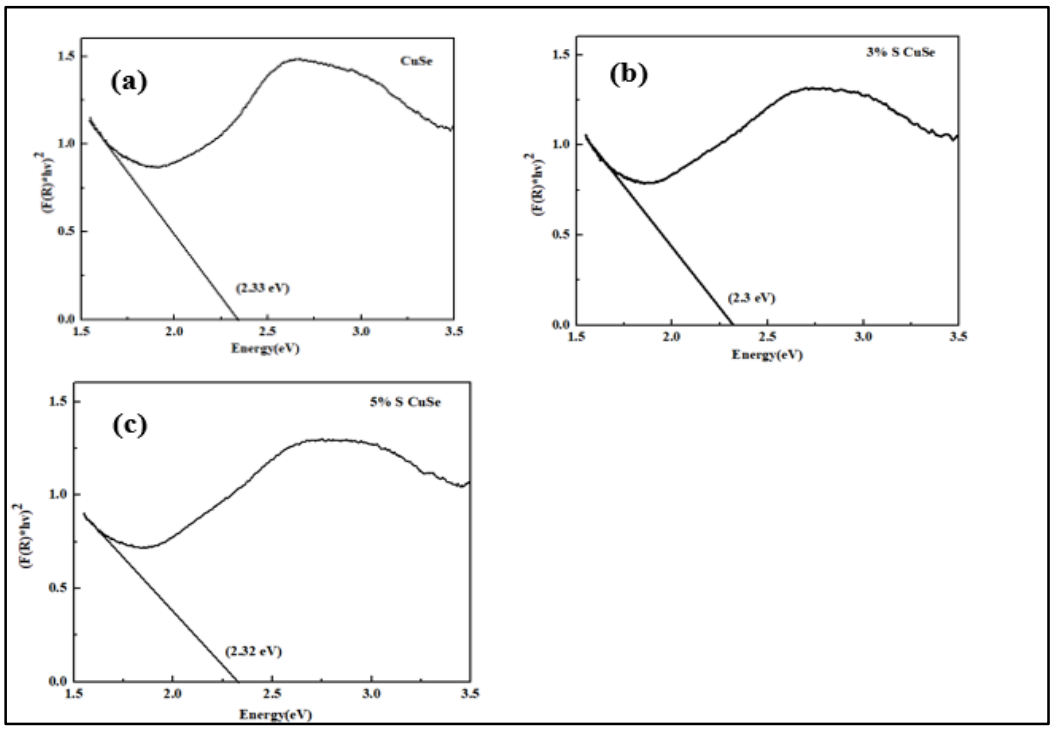

Figure 11: Energy band gap of (a) CuSe, (b) 3% S CuSe, and (c) 5% S CuSe

4.5. Photoluminescence (PL) Analysis

The Photoluminescent (PL) activity of CuSe, 3% S CuSe, and 5% S CuSe are shown in **Figure 12** at room temperature. Photoluminescence emission spectra were mainly intended to investigate the outcome of photogenerated electrons and holes in semiconductors. Since PL emission results from the recombination of free charge carriers, surface vacancies, transfer[106]. The luminescence spectra were collected for an excitation wavelength of 357 nm. The PL spectra of CuSe exhibited a broad main emission peak in the 450 nm region, which was mainly due to the surface defects of CuSe lattice and at around 532 nm. And also the PL spectra of 5% S CuSe exhibited a broad emission peak in the 449 nm region, which might be also due to surface defects of CuSe lattice and at around 532 nm. The PL spectra of 3% S CuSe also exhibited broad emission peaks in the 448 nm region under an excitation wavelength of 357 nm, which was maybe due to the formation of surface defects. Furthermore, the PL intensity of the pristine CuSe and 5% CuSe was almost similar which may be due to the saturation level of the doped sulfur in the copper selenide. And also the PL intensity was exhibited a broad emission peak at 539 nm shows that the photogenerated charge carriers have low efficiency of recombination in 3% S CuSe due to the loading effect of sulfur. Therefore, the enhanced photocatalytic performances of 3% S CuSe can be achieved due to the low efficiency of recombination of hole-electron pairs.

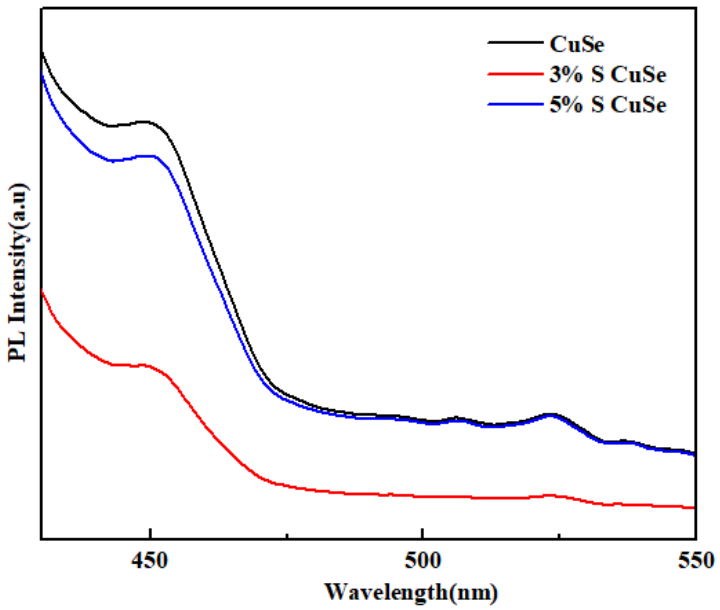

Figure 12 : PL spectra of synthesized CuSe, 3% S CuSe, and 5% S CuSe

4.6. Photocatalytic Activities of the synthesized CuSe and $CuSe_{1-x}S_x$

To study the photocatalytic activity of the synthesized CuSe and $CuSe_{1-x}S_x$, the experiments of photocatalytic degradations of MB solution under a 150 W light source visible light irradiation have been performed. **Figures 13 (a)-(c)** indicate the photocatalytic performance of CuSe, 3% S CuSe, and 5% S CuSe catalysts towards the MB dye. Photocatalysis refers to the oxidation and reduction reactions on semiconductor surfaces, mediated by the valance band holes and conduction band electrons, which are generated by the absorption of visible light radiation. In a typical experiment, 0.05 g of CuSe was dissolved in 100 mL aqueous solutions of MB. As seen in **Figure 13 (a-c)**, a substantial decrease in the absorbance of dye (MB) was observed after conducting the reaction under the catalyst in the dark and after visible light irradiation.

The efficiency of degradation (η %) was calculated using

$$\eta\ (\%) = \left(1 - \frac{At}{A_o}\right) \times 100 \qquad (3)$$

Where A_0 represents the initial concentration of the dye present in the solution and A_t denotes the concentration at any time after irradiation.

Figure 13 (a-c) shows the decrease in the intensity of the 664 nm absorption peak was followed and evaluated to study the degradation of methylene blue under visible light over different time intervals. As the irradiation time increases, the peak at 664 nm declines in intensity indicating the degradation of MB. Upon further light exposure, the absorption peak intensity drops slightly with time. The photocatalytic performance of CuSe, 3% S CuSe, and 5% S CuSe was examined by the degradation of MB as shown in **Figure 13 (d).** 3% S CuSe shows superior photocatalytic performance compared with all samples for the degradation of MB, which degraded 46% of MB in 60 min. **Figure 13 (b)** shows the 3% S CuSe has a high dye adsorption ability during dark reaction due to its bandgap which increases the light-absorbing and decreases the photo recombination lifetime that increases to absorb MB.

The CuSe shows low photocatalytic performance as shown in **Figure 13 (a)** due to its photo-generated charge carrier recombination and optical band gap, which degrades 32% of MB. Strikingly, doping had improved the degradation efficiency of MB. Therefore, the photocatalytic activities of the sulfur-doped copper selenide were higher than that of pure CuSe particles.

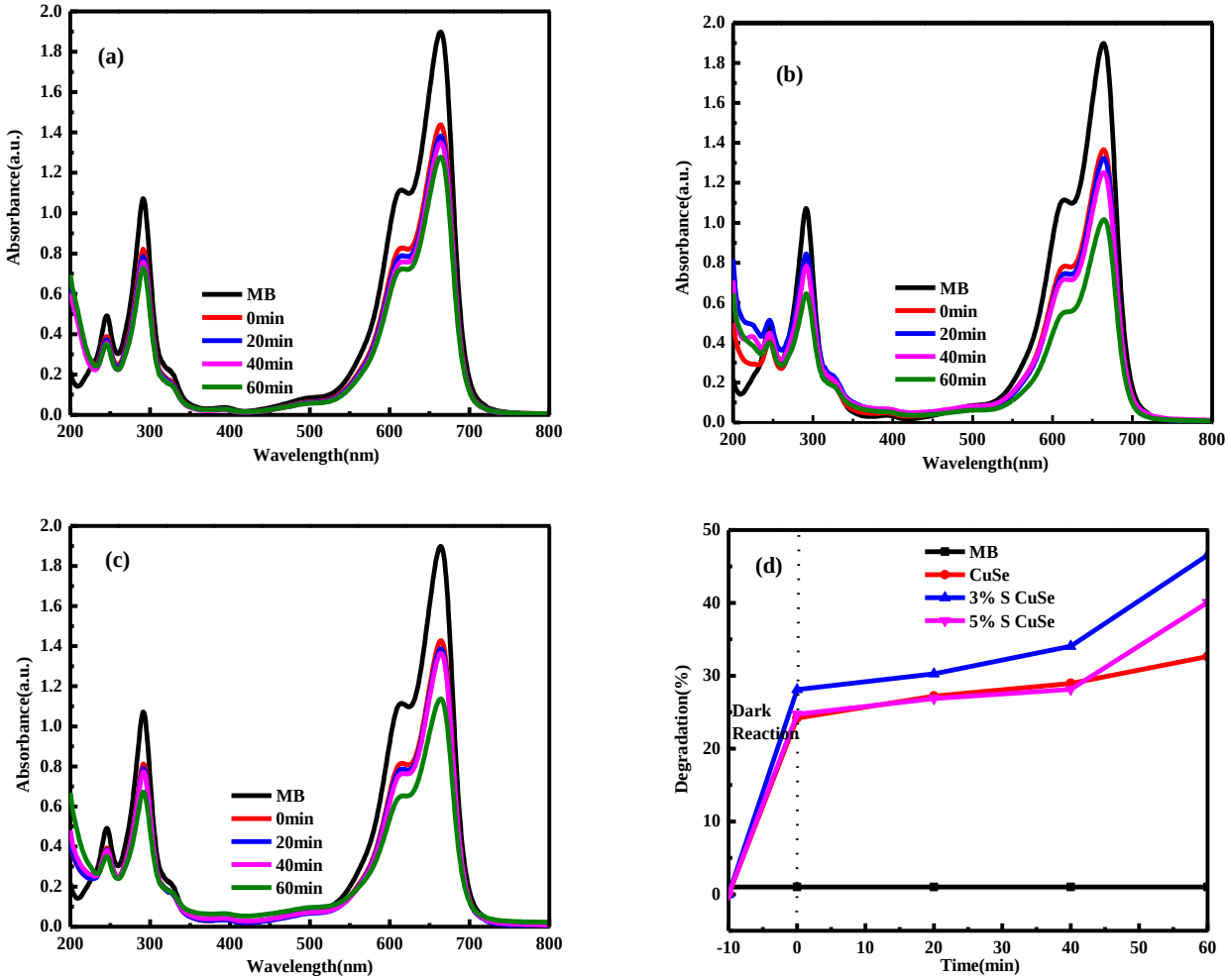

Figure 13: Time-dependent absorption spectra of MB dye in presence of (a) CuSe, (b) 3% S CuSe, and (c) 5% S CuSe catalysts, and (d) Degradation efficiency versus irradiation time

As can be seen from **Figure 14(a)** the photo degradation rates of MB were good with 3% S CuSe. This shows the changes in MB concentration ratio (A_t/A_o) as a function of illumination time. **Figure 14 (b)** shows that the degradation percentage increases as the UV-vis irradiation time increases.

The photocatalytic degradation of the organic dyes by the CuSe under visible light obeyed pseudo-first-order kinetics concerning the absorption intensity of dyes:

$$-\frac{dA}{dt} = \text{kappA} \qquad (4)$$

Integration of the equation (with A = Aabs at t = 0, with Aabs being the initial concentration in the bulk solution after dark adsorption and t the reaction time) lead to

$$-\ln\left(\frac{A}{A^{o}}\right) = \text{Kapp } t \qquad (5)$$

Where A and A^{o} are the absorption intensities at time t = t and t = 0 respectively, Kapp and t are the apparent reaction rate constant and time.

The kinetic degradation of MB dye photodegradation at neutral pH using copper selenide was studied based on pseudo-first-order modal as in equation.

$$-\frac{\ln Ct}{Co} = kt \qquad (6)$$

Where C_t is the concentration of MB at irradiation time t, C_o is the initial concentration, K is the first-order rate constant (min^{-1}).

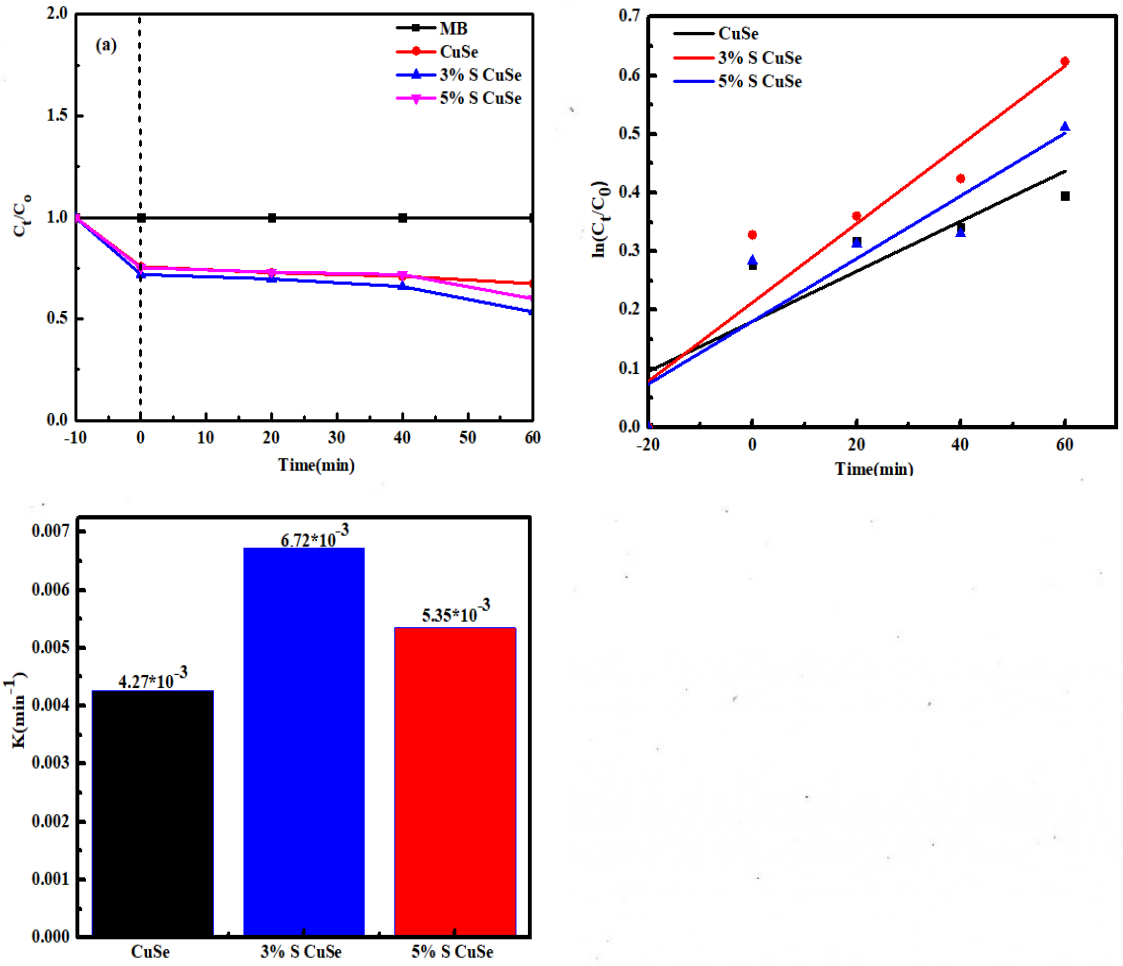

Figure 14: a) The Ct/Co versus irradiation time plot for the MB degradation over CuSe, 3% S CuSe, and 5% CuSe catalysts (b) The first-order kinetic plot and (c) The reaction rate constant of CuSe, 3% S CuSe, and 5% S CuSe catalyst

The plotting ln (C_t/C_o) vs t is shown in **Figure 14** and the value of reaction rate is exhibited in **Figure (b)**. The value of the reaction rate is exhibited in **Figure (c)**. The data fitted well and gave a correlation coefficient of CuSe, 3% S CuSe, and 5% S CuSe to be 0.00427, 0.00672, and 0.00523 for neutral pH respectively. 3% S CuSe presents a higher kinetic rate than pure CuSe.

4.6.2 Effect of Temperature for the removal of MB in Aqueous Solution

Many factors can significantly influence the photocatalytic reaction, such as initial concentration, pH values, the grain size of photocatalysts, specific surface area, morphologies of photocatalysts, and incident light intensity. Those factors have been studied deeply and extensively up to now. However, the effect of system temperature on photocatalysts has not attracted enough attention. In the present research, it is found that temperature affects the photodegradation of methyl blue. To evaluate the effect of temperature on methylene blue degradation the temperature of the solution temperature was changed from room temperature to 50℃, 70℃, and 90℃ for 3% S CuSe by using an electromagnetic heater while other parameters are kept constant. The result was shown in **Figure 15**. Generally, when the reaction temperature increase there is also an increase in photocatalytic reaction. However, reaction temperature above the optimum degree promotes the recombination of the charge carriers and dis-favors the adsorption of the organic compound on the catalyst surface. A reaction temperature below 0℃ results in an increase in the apparent activation energy [50]. As we, increase the temperature there was a formation of a bubble in the solution, which causes the formation of free radicals. So as we increase the temperature this may increase the oxidation rate of dye at the interface. The degradation efficiency of dyes gradually increases with an increase of temperature; the bubbles of solution rose to cause the production of free radicals. Furthermore, the increase in temperature helped the reaction to compete for more efficiency with electron-hole recombination [51]. At a temperature of 70℃, the degradation efficiency is maximum, with the corresponding results of 70 % removal of MB, and decrease at 90 ℃. Therefore, temperature affects the photodegradation of methyl blue.

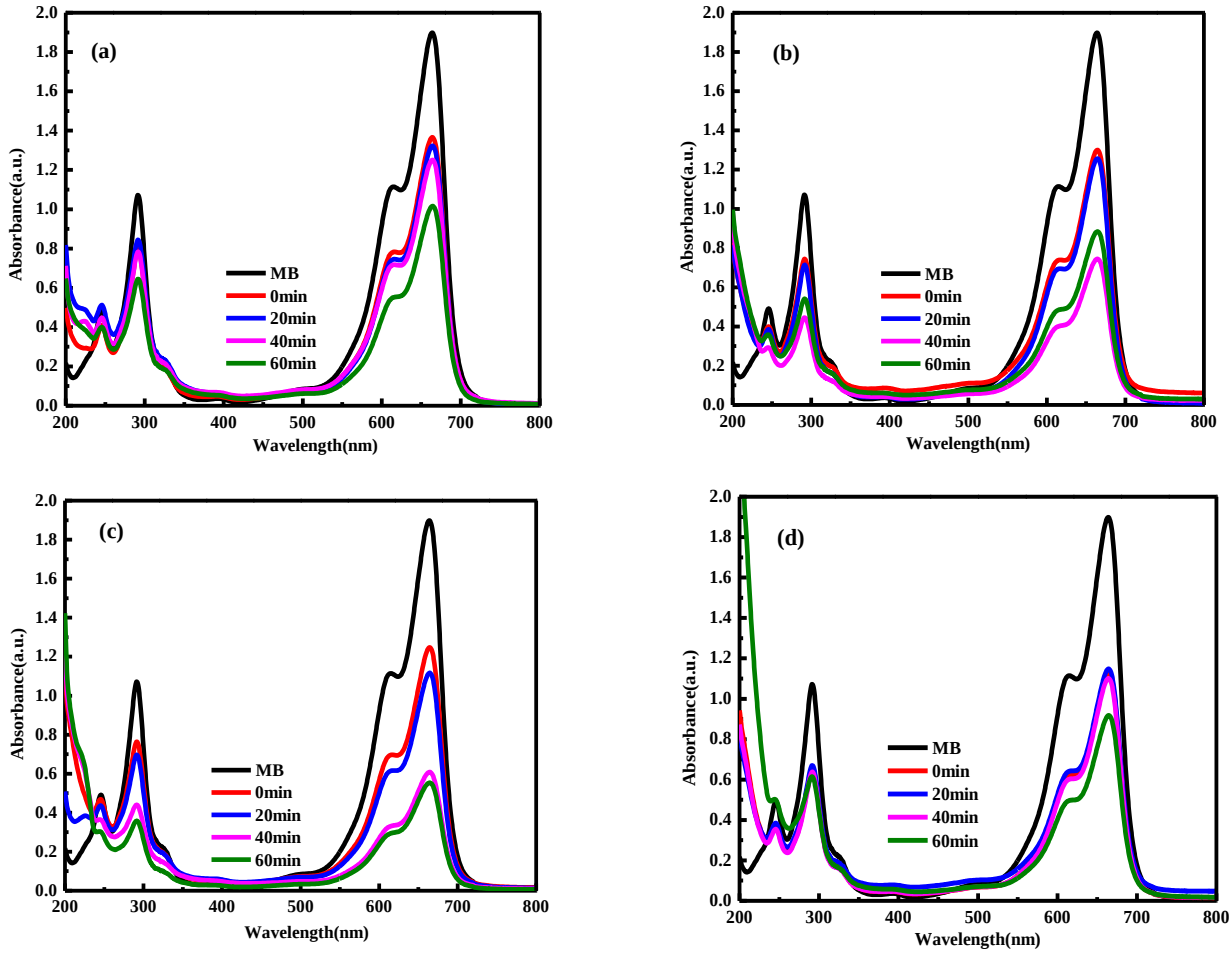

Figure 15: Temperature effect on the time-dependent absorption spectra of MB dye in presence of 3% S CuSe at (a) Room T°, (b) 50℃, (c) 70℃, and (d) 90℃

4.6.3 Kinetics Study for the Effect of Temperature

As can be seen from **Figure 16** the photodegradation rates of MB were good with 3% S CuSe at 70 ℃ under the same condition. The kinetic degradation of MB dye photodegradation at neutral pH using copper selenide was studied based on pseudo-first-order modal as in equation.

$$-\frac{\ln Ct}{Co} = kt \qquad (6)$$

Where C_t is the concentration of MB at irradiation time t, Co is the initial concentration, K is the first-order rate constant (min^{-1}).

The plotting ln (C_t/C_o) vs t is shown in Figure 16 and the value of reaction rate is exhibited in **Figure (b)**. Then plotting ln (C_t/C_o) vs t as shown in and the value of reaction rate is exhibited in **Figure (b)** was calculated for 3% S CuSe, at the room, 50℃, 70℃ and 90℃. The data fitted well and gave a correlation coefficient of 3% S CuSe, at the room, 50℃, 70℃, and 90℃ to be 0.00747, 0.01254, 0.01747, and 0.00801 for neutral pH respectively.

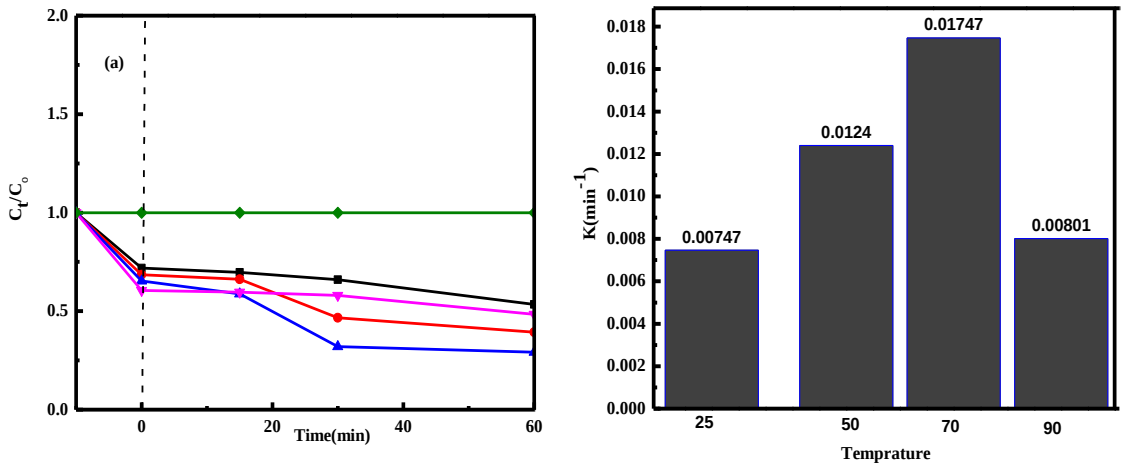

Figure 16: (a) The Ct/Co versus irradiation time plot for the MB degradation over 3% S CuSe at room, 50℃, 70℃, and 90℃ (b) The reaction rate constant of 3% S CuSe

4.7. Temperature-Dependent Photoluminescence (PL)

Figure **17** shows the temperature-dependent PL spectra of 3% S CuSe solution measured at a temperature from the room – 90 ℃ in steps of 20 ℃. The luminescence spectra were collected for an excitation wavelength of 357 nm. The intensity of the emission spectra changes significantly when the temperature rises from the room – 90 ℃. To see the intensity of the spectrum more clearly, the emission spectra are presented in **Figure 17** with various temperatures, respectively. The PL spectrum at the T room exhibits two broad emission peaks, P1 and P2, at wavelengths of 458 nm and 485 nm respectively. It clearly shows that the intensity of the emission at 458 nm and the emission of 485 nm decreases slightly when the temperature rises from the room – 90 ℃ showing a typical thermal quenching behavior. Furthermore, the PL intensity as temperature increase exhibited that the photogenerated charge carriers have low efficiency of recombination in 3% S CuSe due to this temperature effect. Therefore, the increase in temperature helped the reaction to compete for more efficiency with electron-hole recombination [41].

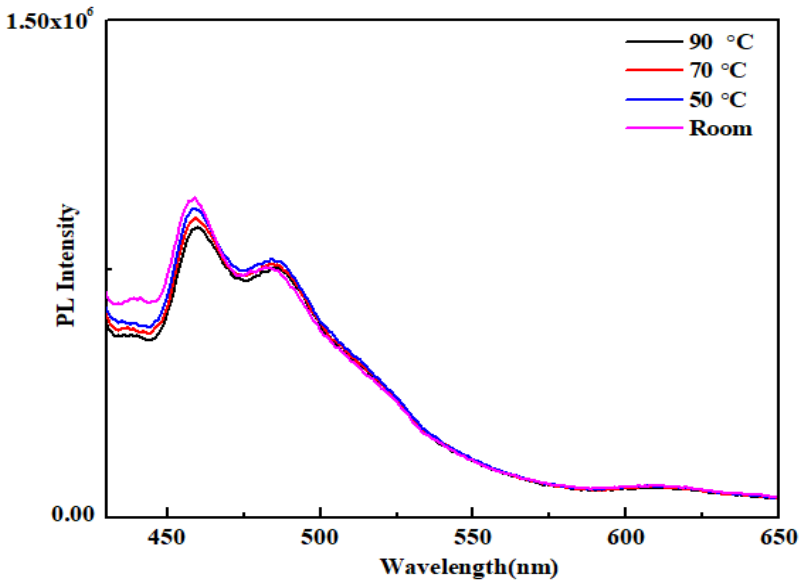

Figure 17 :Temperature dependent photoluminescence (PL)

4.8. Organic Dye Degradation Mechanism of $CuSe_{1-x}S_x$

Doping means the introduction of impurities into a semiconductor crystal to the defined modification of conductivity [126]. The dopant is integrated into the lattice structure of the semiconductor crystal the number of outer electrons defines the type of doping. Doping is an important mechanism in tuning the energy bandgap of the material. So when the bandgap of the semiconductor is reduced then there is a high light absorptive capacity for the material [127]. Non-metal anion doping in CuSe is widely used to hinder the recombination of photogenerated electron/hole and enhance the photocatalytic activity and shift the spectral response to the visible region due to its electronic states. Non-metal anion doped CuSe indicates the bandgap narrow and enhances the absorption of visible light. Various studies were reported and corresponding mechanisms have been proposed to explain the effect on the light adsorption and photocatalytic of non-metal anion doped CuSe. The bandgap of photocatalytic is decreased by sulfur doping. This is due to the change in lattice parameters and due to the trap states within the conduction band (CB) and valence band (VB). As seen in the Figure 18 sulfur has an equivalent atomic size to selenium.

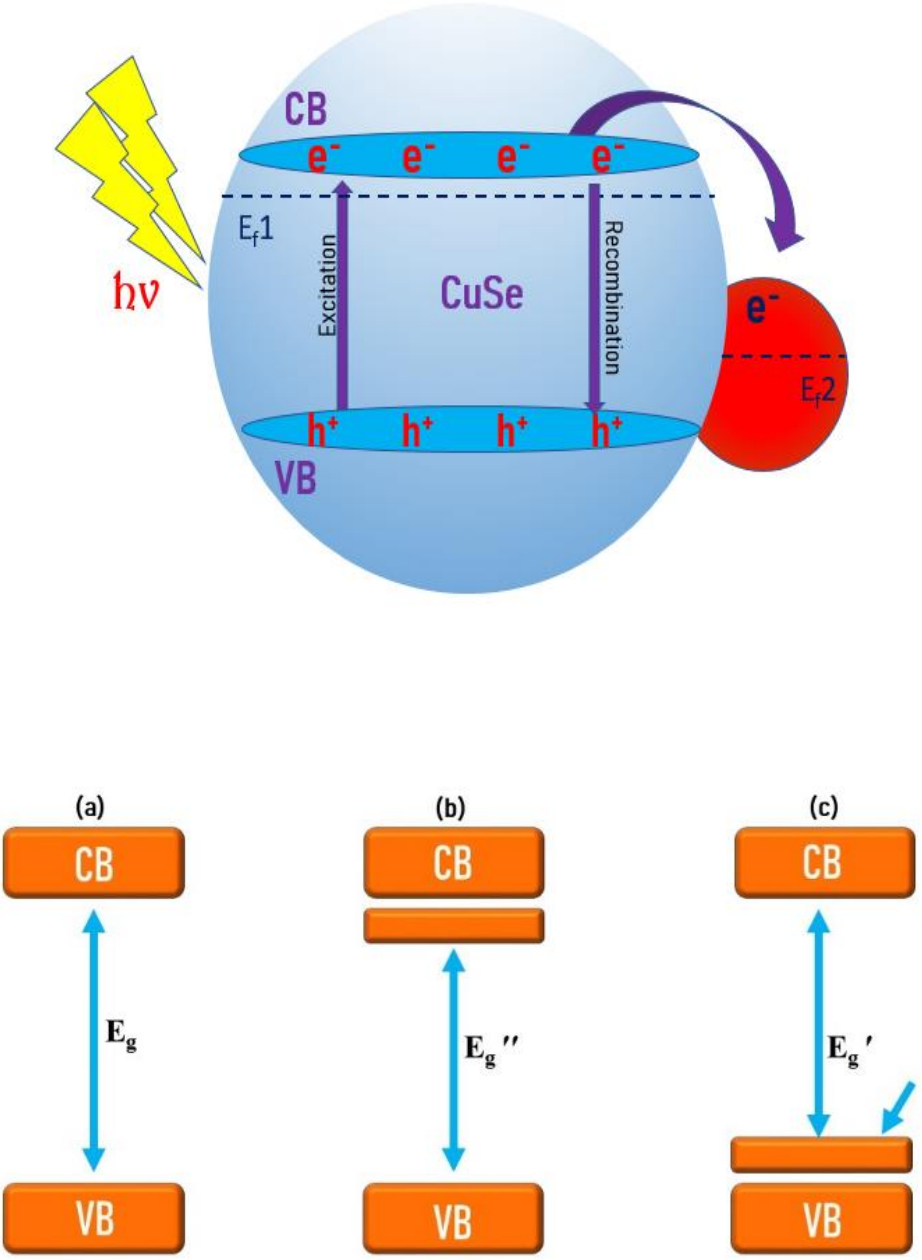

Figure 18: Dye Degradation Mechanism of CuSe1-xSx

4.9. Reusability of the Catalyst

The 3% S CuSe was tested for up to four cycles for the reuse of Methylene blue (MB) aqueous solution as shown in Figure 19. The reusability of sulfur-doped copper selenide catalyst was tested by separating the catalyst by centrifugation, washing with distilled water to remove any adsorbent organic dye, and drying in an oven. The catalyst stability was tested for four cycles. The Figure shows that up to 46% of MB is degraded after 60 min in the first cycle of degradation and MB degradation could be observed in the second to fourth cycles was 45%, 42 %, and 39%, respectively. Thus, the efficiencies for the photodegradation of the photocatalyst in the CuSe photocatalyst are almost similar to MB dye degradation. Reused in four cycles are nearly the same.

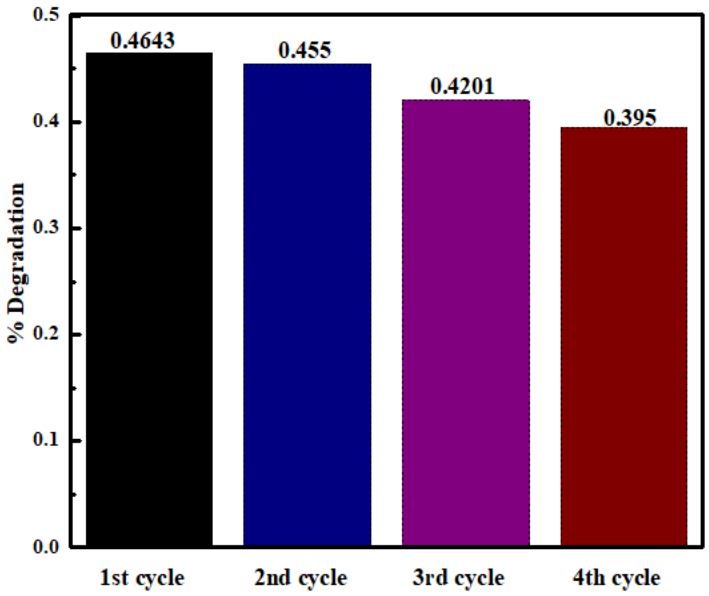

Figure 19: The reusability of 3% S CuSe for degradation of MB degradation.

5. Conclusions and Recommendations

5.1 Conclusion

In this study, CuSe, 3% S CuSe, and 5% S CuSe were successfully synthesized by hydrothermal methods. Then the synthesized materials were characterized using XRD, SEM, FTIR, PL, and UV–vis spectrophotometer to determine phase purity, the particles morphology, functional groups, photon recombination, and the degradation efficiency respectively. From the XRD diffraction pattern, it is confirmed the synthesized CuSe was crystalline klomannite hexagonal with no other impurities peaks and SEM reveals that synthesized pristine CuSe with smooth surface and relatively symmetrical hexagonal shapes. Among them, 3% S CuSe showed a better degradation efficiency at an initial MB concentration of 10 mg/L and a catalyst dose of 0.05g. The effect of temperature ranging from the room - 90℃ was investigated for the present material. At a temperature of 70℃, the degradation efficiency is maximum, with the corresponding results of 70 % removal of MB, and decrease at 90 ℃. Kinetics models were studied for the 3% S CuSe with a time range from 0–60 min and obeyed the Pseudo-first-order degradation kinetics. And also temperature is one of the parameters which greatly affect the catalytic activity of materials, when the reaction temperature increase there is also an increase in photocatalytic reaction. Temperature-dependent Photoluminescence spectra of 3% S CuSe solution measured at a temperature from the room – 90 ℃ in steps of 20 ℃. It clearly shows that the intensity of the emission at 458 nm and the emission of 485 nm decreases slightly when the temperature rises from the room – 90 ℃ showing a typical thermal quenching behavior. Finally, the reusability was studied for up to four cycles and has reusability of 46.5,45.2,42.02 and 39.5 respectively this showed suitable reusability towards the Methylene dye removal.

5.2 Recommendations

In this study, the effect of temperature is investigated on Cu (Se, S) for the degradation of methylene blue in an aqueous solution. The results show that temperature is one of the parameters, which greatly affects photocatalytic activity. We further recommend the investigation of the temperature effect towards other toxic organic dyes such as MO, RhB, Congo red, and so on. Further characterization is needed to prove the elemental composition for the CuSe and sulfur doped CuSe. Therefore, for the determination of doping and elemental composition XPS and EDX are recommended respectively.

REFERENCE

1. Shojaei, A.R., et al., *Ab initio investigation of the structural and unusual electronic properties of α-CuSe (klockmannite).* Chinese Physics B, 2013. 22(12): p. 127102.
2. Milman, V., *Klockmannite, CuSe: structure, properties and phase stability from ab initio modeling.* Acta Crystallographica Section B: Structural Science, 2002. 58(3): p. 437-447.
3. Kodali, R.K., B. Kirti, and L. Boppana. *IoT based Water Management System*. in *2021 International Conference on Computer Communication and Informatics (ICCCI)*. 2021. IEEE.
4. Berdalet, E., et al., *Marine harmful algal blooms, human health and wellbeing: challenges and opportunities in the 21st century.* Journal of the Marine Biological Association of the United Kingdom, 2016. 96(1): p. 61-91.
5. Odlare, M., *Introductory chapter for water resources.* 2013.
6. Nandhini, N., S. Rajeshkumar, and S. Mythili, *The possible mechanism of eco-friendly synthesized nanoparticles on hazardous dyes degradation.* Biocatalysis and Agricultural Biotechnology, 2019. 19: p. 101138.
7. Hasanpour, M. and M. Hatami, *Photocatalytic performance of aerogels for organic dyes removal from wastewaters: Review study.* Journal of Molecular Liquids, 2020. 309: p. 113094.
8. Burleson, D.J., M.D. Driessen, and R.L. Penn, *On the characterization of environmental nanoparticles.* Journal of Environmental Science and Health, Part A, 2004. 39(10): p. 2707-2753.
9. Ali, H., *Biodegradation of synthetic dyes—a review.* Water, Air, & Soil Pollution, 2010. 213(1): p. 251-273.
10. Lellis, B., et al., *Effects of textile dyes on health and the environment and bioremediation potential of living organisms.* Biotechnology Research and Innovation, 2019. 3(2): p. 275-290.
11. Benkhaya, S., S. M'rabet, and A. El Harfi, *A review on classifications, recent synthesis and applications of textile dyes.* Inorganic Chemistry Communications, 2020. 115: p. 107891.
12. Panda, H., *A concise guide on textile dyes, pigments and dye intermediates with textile printing technology*. 2013: Niir Project Consultancy Services.

13. Ding, Y. and H.S. Freeman, *Mordant dye application on cotton: optimisation and combination with natural dyes.* Coloration Technology, 2017. 133(5): p. 369-375.
14. Landolt, A., *The action of light on cellulose dyed with vat dyes.* Journal of the Society of Dyers and Colourists, 1949. 65(12): p. 659-673.
15. Waring, D.R., *Dyes for cellulosic fibers*, in *The Chemistry and Application of Dyes*. 1990, Springer. p. 49-106.
16. Iskender, M.A., B. Becerir, and A. Koruyucu, *Carrier dyeing of different energy level disperse dyes on polyester fabric.* Textile Research Journal, 2005. 75(6): p. 462-465.
17. Kumar, R., *Preparation characterization and adsorption studies of adsorbents for dyes removal*. 2011, Aligarh Muslim University.
18. Dikshit, R. and P. Tallapragada, *Comparative study of natural and artificial flavoring agents and dyes*, in *Natural and artificial flavoring agents and food dyes*. 2018, Elsevier. p. 83-111.
19. Al-Ghouti, M.A. and R.S. Al-Absi, *Mechanistic understanding of the adsorption and thermodynamic aspects of cationic methylene blue dye onto cellulosic olive stones biomass from wastewater.* Scientific Reports, 2020. 10(1): p. 1-18.
20. Rafiq, A., et al., *Photocatalytic and catalytic degradation of organic dye by uncapped and capped ZnS quantum dots.* Materials Research Express, 2019. 6(5): p. 055801.
21. Rajamani, M. and K. Rajendrakumar, *Chitosan-boehmite desiccant composite as a promising adsorbent towards heavy metal removal.* Journal of environmental management, 2019. 244: p. 257-264.
22. Crini, G. and E. Lichtfouse, *Advantages and disadvantages of techniques used for wastewater treatment.* Environmental Chemistry Letters, 2019. 17(1): p. 145-155.
23. Oller, I., S. Malato, and J. Sánchez-Pérez, *Combination of advanced oxidation processes and biological treatments for wastewater decontamination—a review.* Science of the total environment, 2011. 409(20): p. 4141-4166.
24. Mouele, E.S.M., et al., *Degradation of organic pollutants and microorganisms from wastewater using different dielectric barrier discharge configurations—a critical review.* Environmental Science and Pollution Research, 2015. 22(23): p. 18345-18362.
25. Samer, M., *Biological and chemical wastewater treatment processes.* Wastewater treatment engineering, 2015. 150.
26. Ahmad, A., et al., *Recent advances in new generation dye removal technologies: novel search for approaches to reprocess wastewater.* RSC advances, 2015. 5(39): p. 30801-30818.

27. El-Gendy, A., et al., *Carbon-based materials (CBMS) for determination and remediation of antimicrobials in different substrates: Wastewater and infant foods as examples.* Carbon-Based Material for Environmental Protection and Remediation; Bartoli, M., Frediani, M., Rosi, L., Eds, 2020: p. 103-122.
28. Joseph, C.G., et al., *Sonophotocatalysis in advanced oxidation process: a short review.* Ultrasonics Sonochemistry, 2009. 16(5): p. 583-589.
29. Kanakaraju, D., B.D. Glass, and M. Oelgemöller, *Advanced oxidation process-mediated removal of pharmaceuticals from water: a review.* Journal of environmental management, 2018. 219: p. 189-207.
30. Kowalska, E., et al., *Noble metal nanoparticles for water purification*, in *Nanoscale materials in water purification*. 2019, Elsevier. p. 553-579.
31. Guerra-Rodríguez, S., et al., *Assessment of sulfate radical-based advanced oxidation processes for water and wastewater treatment: a review.* Water, 2018. 10(12): p. 1828.
32. Ghosh, I., et al., *Organic semiconductor photocatalyst can bifunctionalize arenes and heteroarenes.* Science, 2019. 365(6451): p. 360-366.
33. Algesheimer, R., U.M. Dholakia, and A. Herrmann, *The social influence of brand community: Evidence from European car clubs.* Journal of marketing, 2005. 69(3): p. 19-34.
34. Cieśla, P., et al., *Homogeneous photocatalysis by transition metal complexes in the environment.* Journal of Molecular Catalysis A: Chemical, 2004. 224(1-2): p. 17-33.
35. Fox, M.A. and M.T. Dulay, *Heterogeneous photocatalysis.* Chemical reviews, 1993. 93(1): p. 341-357.
36. Koe, W.S., et al., *An overview of photocatalytic degradation: photocatalysts, mechanisms, and development of photocatalytic membrane.* Environmental Science and Pollution Research, 2020. 27(3): p. 2522-2565.
37. Anwer, H., et al., *Photocatalysts for degradation of dyes in industrial effluents: Opportunities and challenges.* Nano Research, 2019. 12(5): p. 955-972.
38. Pelaez, M., et al., *A review on the visible light active titanium dioxide photocatalysts for environmental applications.* Applied Catalysis B: Environmental, 2012. 125: p. 331-349.
39. Hoertz Jr, P.G., *Charge separation and recombination in dye-sensitized nanocrystalline titanium dioxide films*. 2004: The Johns Hopkins University.

40. Sarina, S., E.R. Waclawik, and H. Zhu, *Photocatalysis on supported gold and silver nanoparticles under ultraviolet and visible light irradiation.* Green Chemistry, 2013. 15(7): p. 1814-1833.
41. Saravanan, R., F. Gracia, and A. Stephen. *Chapter 2 Basic Principles , Mechanism , and Challenges of Photocatalysis*. 2017.
42. Hoffmann, M.R., et al., *Environmental applications of semiconductor photocatalysis.* Chemical reviews, 1995. 95(1): p. 69-96.
43. Su, Y., et al., *Surface hydrogen bonds assisted meso-porous WO3 photocatalysts for high selective oxidation of benzylalcohol to benzylaldehyde.* Applied Catalysis B: Environmental, 2017. 217: p. 108-114.
44. Tyagi, K., et al., *Band structure and transport studies of copper selenide: An efficient thermoelectric material.* Applied Physics Letters, 2014. 105(17): p. 173905.
45. Pignatello, J.J., E. Oliveros, and A. MacKay, *Advanced oxidation processes for organic contaminant destruction based on the Fenton reaction and related chemistry.* Critical reviews in environmental science and technology, 2006. 36(1): p. 1-84.
46. Reza, K.M., A. Kurny, and F. Gulshan, *Parameters affecting the photocatalytic degradation of dyes using TiO 2: a review.* Applied Water Science, 2017. 7(4): p. 1569-1578.
47. Azad, K. and P. Gajanan, *Photodegradation of methyl orange in aqueous solution by the visible light active Co: La: TiO2 nanocomposite.* Chem. Sci. J, 2017. 164.
48. Kumar, A. and G. Pandey, *A review on the factors affecting the photocatalytic degradation of hazardous materials.* Mater. Sci. Eng. Int. J, 2017. 1(3): p. 1-10.
49. Heidari, S., M. Haghighi, and M. Shabani, *Sunlight-activated BiOCl/BiOBr–Bi24O31Br10 photocatalyst for the removal of pharmaceutical compounds.* Journal of Cleaner Production, 2020. 259: p. 120679.
50. Umar, M. and H.A. Aziz, *Photocatalytic degradation of organic pollutants in water.* Organic pollutants-monitoring, risk and treatment, 2013. 8: p. 196-197.
51. Karimi, L., S. Zohoori, and M.E. Yazdanshenas, *Photocatalytic degradation of azo dyes in aqueous solutions under UV irradiation using nano-strontium titanate as the nanophotocatalyst.* Journal of Saudi Chemical Society, 2014. 18(5): p. 581-588.
52. Rueggeberg, F., W.F. Caughman, and J. Curtis Jr, *Effect of light intensity and exposure duration on cure of resin composite.* Operative dentistry, 1994. 19(1): p. 26-32.
53. Pareek, V., et al., *Light intensity distribution in heterogenous photocatalytic reactors.* Asia-Pacific Journal of Chemical Engineering, 2008. 3(2): p. 171-201.

54. Seeger, K., *Semiconductor physics*. 2013: Springer Science & Business Media.
55. Daude, N., C. Gout, and C. Jouanin, *Electronic band structure of titanium dioxide.* Physical Review B, 1977. 15(6): p. 3229.
56. Saranya, M., et al., *Enhanced visible light photocatalytic reduction of organic pollutant and electrochemical properties of CuS catalyst.* Powder Technology, 2015. 279: p. 209-220.
57. Trindade, T., P. O'Brien, and N.L. Pickett, *Nanocrystalline semiconductors: synthesis, properties, and perspectives.* Chemistry of Materials, 2001. 13(11): p. 3843-3858.
58. Ajmal, A., et al., *Principles and mechanisms of photocatalytic dye degradation on TiO 2 based photocatalysts: a comparative overview.* Rsc Advances, 2014. 4(70): p. 37003-37026.
59. Muruganandham, M. and M. Swaminathan, *Solar photocatalytic degradation of a reactive azo dye in TiO2-suspension.* Solar Energy Materials and Solar Cells, 2004. 81(4): p. 439-457.
60. Rahman, Q.I., et al., *Effective photocatalytic degradation of rhodamine B dye by ZnO nanoparticles.* Materials Letters, 2013. 91: p. 170-174.
61. Chen, X., et al., *Preparation of ZnO photocatalyst for the efficient and rapid photocatalytic degradation of azo dyes.* Nanoscale research letters, 2017. 12(1): p. 1-10.
62. Szilágyi, I.M., et al., *WO3 photocatalysts: Influence of structure and composition.* Journal of catalysis, 2012. 294: p. 119-127.
63. Cui, Y., et al., *Synthesis of novel 3D SnO flower-like hierarchical architectures self-assembled by nano-leaves and its photocatalysis.* Materials Research Bulletin, 2015. 70: p. 784-788.
64. Chen, X., et al., *In situ construction of an SnO 2/gC 3 N 4 heterojunction for enhanced visible-light photocatalytic activity.* Rsc Advances, 2015. 5(84): p. 68953-68963.
65. Ye, Z., et al., *A comparative study of photocatalytic activity of ZnS photocatalyst for degradation of various dyes.* Optik, 2018. 164: p. 345-354.
66. Sivakumar, P., G.G. Kumar, and S. Renganathan, *Synthesis and characterization of ZnS-Ag nanoballs and its application in photocatalytic dye degradation under visible light.* Journal of Nanostructure in Chemistry, 2014. 4(3): p. 1-9.
67. Borhade, A. and B. Uphade, *A comparative study on characterization and photocatalytic activities of PbS and Co doped PbS nanoparticles.* Chalcogenide Lett, 2012. 9(7): p. 299-306.

68. Ratanatawanate, C., Y. Tao, and K.J. Balkus Jr, *Photocatalytic activity of PbS quantum dot/TiO2 nanotube composites.* The Journal of Physical Chemistry C, 2009. 113(24): p. 10755-10760.
69. Das, D. and R.K. Dutta, *A novel method of synthesis of small band gap SnS nanorods and its efficient photocatalytic dye degradation.* Journal of colloid and interface science, 2015. 457: p. 339-344.
70. Ayodhya, D., et al., *Photocatalytic degradation of dye pollutants under solar, visible and UV lights using green synthesised CuS nanoparticles.* Journal of Experimental Nanoscience, 2016. 11(6): p. 418-432.
71. Saranya, M., et al., *Hydrothermal growth of CuS nanostructures and its photocatalytic properties.* Powder technology, 2014. 252: p. 25-32.
72. Ayodhya, D. and G. Veerabhadram, *A review on recent advances in photodegradation of dyes using doped and heterojunction based semiconductor metal sulfide nanostructures for environmental protection.* Materials today energy, 2018. 9: p. 83-113.
73. Chang, J. and E.R. Waclawik, *Colloidal semiconductor nanocrystals: controlled synthesis and surface chemistry in organic media.* RSC Advances, 2014. 4(45): p. 23505-23527.
74. Zhu, T., et al., *Arrays of ultrafine CuS nanoneedles supported on a CNT backbone for application in supercapacitors.* Journal of Materials Chemistry, 2012. 22(16): p. 7851-7855.
75. Chen, Y., et al., *Growth of single-crystal copper sulfide thin films via electrodeposition in ionic liquid media for lithium ion batteries.* Journal of Materials Chemistry, 2012. 22(12): p. 5295-5299.
76. Lei, H., et al., *Enhanced efficiency in organic solar cells via in situ fabricated p-type copper sulfide as the hole transporting layer.* Solar energy materials and solar cells, 2014. 128: p. 77-84.
77. Dong, H., et al., *Colloidally stable selenium@ copper selenide core@ shell nanoparticles as selenium source for manufacturing of copper–indium–selenide solar cells.* Journal of colloid and interface science, 2014. 415: p. 103-110.
78. Zaman, M.S., C.H. Moon, and E.D. Haberer, *Sensitive ammonia gas sensors fabricated using biologically assembled copper sulfide.* Applied Physics Express, 2014. 7(11): p. 117002.

79. Hessel, C.M., et al., *Copper selenide nanocrystals for photothermal therapy.* Nano letters, 2011. 11(6): p. 2560-2566.
80. Zha, Z., et al., *Enzyme-responsive copper sulphide nanoparticles for combined photoacoustic imaging, tumor-selective chemotherapy and photothermal therapy.* Chemical Communications, 2013. 49(33): p. 3455-3457.
81. Gu, Y., et al., *Hydrothermal synthesis of hexagonal CuSe nanoflakes with excellent sunlight-driven photocatalytic activity.* CrystEngComm, 2014. 16(39): p. 9185-9190.
82. Tanveer, M., et al., *Template free synthesis of CuS nanosheet-based hierarchical microspheres: an efficient natural light driven photocatalyst.* CrystEngComm, 2014. 16(24): p. 5290-5300.
83. Shamraiz, U., et al., *Functional metal sulfides and selenides for the removal of hazardous dyes from Water.* Journal of Photochemistry and Photobiology B: Biology, 2016. 159: p. 33-41.
84. Xie, X., et al., *Fabrication of a Cu2-xSe/rGO heterojunction photocatalyst to achieve efficient photocatalytic H2 generation.* International Journal of Hydrogen Energy, 2019. 44(60): p. 32042-32053.
85. Sonia, S., et al., *Influence of growth and photocatalytic properties of copper selenide (CuSe) nanoparticles using reflux condensation method.* Applied surface science, 2013. 283: p. 802-807.
86. Hankare, P., et al., *Preparation of copper selenide thin films by simple chemical route at low temperature and their characterization.* Journal of alloys and compounds, 2009. 469(1-2): p. 478-482.
87. Berry, L., *The crystal structure of covellite, cuse and klockmannite, cuse.* American Mineralogist: Journal of Earth and Planetary Materials, 1954. 39(5-6): p. 504-509.
88. Peiris, S.M., T.T. Pearson, and D.L. Heinz, *Compression of klockmannite, CuSe.* The Journal of chemical physics, 1998. 109(2): p. 634-636.
89. Nouri, M., et al., *Tuning crystal phase and morphology of copper selenide nanostructures and their visible-light photocatalytic applications to degrade organic pollutants.* Colloids and Surfaces A: Physicochemical and Engineering Aspects, 2020. 586: p. 124196.
90. Luo, B., G. Liu, and L. Wang, *Recent advances in 2D materials for photocatalysis.* Nanoscale, 2016. 8(13): p. 6904-6920.

91. Sharma, S.D., et al., *Structural, morphological and thermoelectric properties of self-decorated copper selenide nanosheets synthesized at room temperature.* Current Applied Physics, 2020.
92. Ali, N., et al., *Selenide-chitosan as high-performance nanophotocatalyst for accelerated degradation of pollutants.* Chemistry–An Asian Journal, 2020. 15(17): p. 2660-2673.
93. Nouri, M., et al., *High solar-light photocatalytic activity of using Cu3Se2/rGO nanocomposites synthesized by a green co-precipitation method.* Solid State Sciences, 2017. 73: p. 7-12.
94. Hoda, N. and F. Jamali-Sheini, *Influence of synthesis parameters on the physical properties of Cu3Se2 nanostructures using the sonochemical method.* Ceramics International, 2019. 45(14): p. 16765-16775.
95. Nouri, M., et al., *S-doping effects on optical properties and highly enhanced photocatalytic performance of Cu3Se2 nanoparticles under solar-light irradiation.* Ceramics International, 2017. 43(17): p. 14983-14988.
96. Baghchesara, M.A., et al., *Improving the intrinsic properties of rGO sheets by S-doping and the effects of rGO improvements on the photocatalytic performance of Cu3Se2/rGO nanocomposites.* Applied Surface Science, 2019. 466: p. 401-410.
97. Feng, S. and R. Xu, *New materials in hydrothermal synthesis.* Accounts of chemical research, 2001. 34(3): p. 239-247.
98. Rabenau, A., *The role of hydrothermal synthesis in preparative chemistry.* Angewandte Chemie International Edition in English, 1985. 24(12): p. 1026-1040.
99. Goel, P., *Water pollution: causes, effects and control*. 2006: New Age International.
100. Xue, Y., et al., *A simple strategy for selective photocatalysis degradation of organic dyes through selective adsorption enrichment by using a complex film of CdS and carboxylmethyl starch.* Journal of Environmental Management, 2020. 274: p. 111184.
101. Nasir, A.M., et al., *A review on floating nanocomposite photocatalyst: Fabrication and applications for wastewater treatment.* Journal of Water Process Engineering, 2020. 36: p. 101300.
102. Hussain, R.A. and I. Hussain, *Copper selenide thin films from growth to applications.* Solid State Sciences, 2020. 100: p. 106101.
103. Pacoste, L.G.C., *Development of Copper Selenide Quantum Dots-Based Therapeutic Drug Monitoring Biosensors for Toremifene-A Breast Cancer Drug.* 2017.

104. Liu, M.L., et al., *Dendritic CuSe with hierarchical side-branches: synthesis, efficient adsorption, and enhanced photocatalytic activities under daylight.* ACS Sustainable Chemistry & Engineering, 2017. 5(5): p. 4154-4160.
105. Ghobadi, N., et al., *Tuning the optical and photocatalytic features of copper selenide prepared by chemical solution deposition method.* Surfaces and Interfaces, 2020. 21: p. 100706.
106. Kaviyarasu, K., et al., *Solution processing of CuSe quantum dots: Photocatalytic activity under RhB for UV and visible-light solar irradiation.* Materials Science and Engineering: B, 2016. 210: p. 1-9.
107. Singh, S.C., et al., *Structural and compositional control in copper selenide nanocrystals for light-induced self-repairable electrodes.* Nano energy, 2018. 51: p. 774-785.
108. Ni, S., et al., *Bandgap tuning and photocatalytic activities of CuSe1–xSx nanoflakes.* Ceramics International, 2016. 42(1): p. 211-219.
109. Iqbal, M., et al., *Graphene oxide nanocomposite with CuSe and photocatalytic removal of Methyl Green dye under visible light irradiation.* Diamond and Related Materials, 1921: p. 108254.
110. Cho, A., et al., *The growth of Cu2− xSe thin films using nanoparticles.* Thin Solid Films, 2013. 546: p. 299-307.
111. Hou, X., et al., *The study of morphology-controlled synthesis and the optical properties of CuSe nanoplates based on the hydrothermal method.* Materials Science in Semiconductor Processing, 2018. 79: p. 92-98.
112. Rahmati, A. and A. Farokhipour, *Rectifying behaviour and photocatalytic activity in ZnO nanorods array/Ag/CuSe heterostructure.* Journal of Cluster Science, 2019. 30(2): p. 521-529.
113. Bai, M., et al., *Preparation of CuSe-PDA/gC 3 N 4 and its visible-light photocatalytic performance to dye degradation.* Environmental Science and Pollution Research, 2021. 28(3): p. 3465-3474.
114. Gan, Y.X., et al., *Hydrothermal synthesis of nanomaterials*. 2020, Hindawi.
115. Pathak, H., et al., *Naphthalene degradation by Pseudomonas sp. HOB1: in vitro studies and assessment of naphthalene degradation efficiency in simulated microcosms.* Journal of hazardous materials, 2009. 166(2-3): p. 1466-1473.
116. Bindu, P. and S. Thomas, *Optical properties of ZnO nanoparticles synthesised from a polysaccharide and ZnCl2.* Acta Phys. Pol. A, 2017. 131(6): p. 1474-1478.

117. Ezema, F. and R. Osuji, *Band gap shift and optical characterization of chemical bath deposited CdSSe thin films on annealing.* Chalcogenide Letters, 2007. 4(6): p. 69-75.
118. Mao, Y., et al., *Large-scale preparation of fernwort-like single-crystalline superstructures of CuSe as Fenton-like catalysts for dye decolorization.* Science China Chemistry, 2016. 59(7): p. 903-909.
119. Iqbal, M., et al., *Graphene oxide nanocomposite with CuSe and photocatalytic removal of methyl green dye under visible light irradiation.* Diamond and Related Materials, 2021. 113: p. 108254.
120. Wang, D. and L. Wang, *Temperature dependent luminescent characterization of BaMgSiO4: Eu2+ phosphor.* Materialia, 2021. 15: p. 100982.
121. Barroso-Bogeat, A.n., et al., *FT-IR analysis of pyrone and chromene structures in activated carbon.* Energy & fuels, 2014. 28(6): p. 4096-4103.
122. Mokubung, K., M. Moloto, and N. Moloto, *Low temperature synthesis of l-cysteine capped cu2se quantum dots.* Chalcogenide Letters, 2018. 15(11): p. 529-533.
123. Chandran, A., et al., *Vibrational spectroscopic study of (E)-4-(benzylideneamino)-N-carbamimidoyl benzenesulfonamide.* International Scholarly Research Notices, 2012. 2012.
124. Krivanek, O.L., et al., *Vibrational spectroscopy in the electron microscope.* Nature, 2014. 514(7521): p. 209-212.
125. López, R. and R. Gómez, *Band-gap energy estimation from diffuse reflectance measurements on sol–gel and commercial TiO 2: a comparative study.* Journal of sol-gel science and technology, 2012. 61(1): p. 1-7.
126. Liu, W. and M. Asheghi. *Thermal conduction in ultra-thin pure and doped single crystal silicon layers at high temperatures*. in *Heat Transfer Summer Conference*. 2005.
127. Chaves, A., et al., *Bandgap engineering of two-dimensional semiconductor materials.* npj 2D Materials and Applications, 2020. 4(1): p. 1-21.